 CMES, vol.89, no.5, pp.417-458, 2012

SGBEM (Using Non-hyper-singular Traction BIE), and Super Elements, for Non-Collinear Fatigue-growth Analyses of Cracks in Stiffened Panels with Composite-Patch Repairs

Leiting Dong [1,2] **and Satya N. Atluri** [2]

Abstract: Two-dimensional weakly-singular Symmetric Galerkin Boundary Elements (SGBEMs) are developed, following the work of [Han and Atluri (2003)], using non-hypersingular integral equations for tractions. Specifically, the present 2D SGBEM is used to compute the stress intensity factors for arbitrary-shaped line cracks, including embedded, edge, branching, and intersecting cracks. The computed stress intensity factors show high accuracy, even with very coarse meshes. The non-collinear mixed-mode fatigue growth analysis of cracks requires a very minimal effort—simply extending the cracks by adding an element to each crack tip, in the direction of the crack-growth as determined by a physics-based criterion. Moreover, by rearranging the symmetric Galerkin boundary integral equations, a Super Element containing the arbitrarily growing crack is developed. The Super Element is an arbitrarily-shaped domain with or without cracks inside it. Each Super Element has a stiffness matrix and a force vector, which have physical meanings similar to those by traditional finite elements.Likewise, the stiffness matrix of the Super Element is also positive semi-definite and has exactly three rigid body modes. Super Elements can therefore be directly coupled with traditional finite elements, using the simple assembly procedure. Super Elements are thus very suitable for analyzing large-scale structures and complex structures with cracks growing under fatigue. Fatigue analysis of cracked thin panels with stiffeners and composite patches are presented, showing the simplicity and efficiency of using SGBEM Super Elements to model cracked and repaired stiffened aircraft structures.

Keywords: SGBEM, Super Element, crack, stress intensity factor, fatigue, composite structure

[1] Department of Engineering Mechanics, Hohai University
[2] Center for Aerospace Research & Education, University of California, Irvine

1 Introduction

Understanding the mechanical behavior of solids and structures from both top-down and bottom-up, in various scales, is one of the most important tasks in engineering and science. While some of the behaviors are relatively simple, others frequently involve displacement/stress/strain fields with discontinuities, high gradients, and singularities. One typical example is to study the fracture and fatigue behavior of cracks, which remains an important task in the structural integrity assessment and damage tolerance analysis [Atluri(1998)].

Finite element method is one of the most widely-used computational tools, due to its theoretical simplicity and the many available commercial finite element codes. When modeling facture mechanics problems, hybrid crack-tip elements by [Tong, Pian and Lasry (1973); Atluri, Kobayashi and Nakagaki (1975)] and isoperimetric quarter-point elements by [Henshell andShaw (1975)] are frequently used to capture the crack-tip singularity. Path-independent integrals [Rice (1968); Atluri (1982); Nishioka and Atluri (1983)], and domain-independent integrals [Nikishkov and Atluri (1987)] are almost always used together with finite elements, in order to obtain relatively accurate stress intensity factors. A large number of related works were recorded in [Atluri (1986)]. However, the need of continuous remeshing makes the fatigue analysis with finite elementsvery difficult.

The later method of XFEM, e.g. [Moes, Dolbow and Belytschko (1999)], while becoming very popular in the past decade, however, differs very little from the embedded-singularity elements developed in the 1970s and cited above. Both the widely popular XFEM of the past decade, and the enriched elements of the 1970s, use crack-tip singular fields to enrich the trial functions. However, singular enrichment is limited only to the elements which are immediately adjacent to the crack-tip/crack-front. Therefore, for elements near the crack tip/ crack-front, but not immediately adjacent to the crack tip/ crack front, a very fine and good-quality mesh is still necessary to capture the high gradients of the stress field.

In a totally different way, after the derivation of analytical solutions of elliptical cracks with arbitrary surface tractions, the first paper on a Finite Element Alternating Method (FEAM) was published in [Nishioka and Atluri (1983)]. In Nishioka and Atluri (1983), the analytical solutions for an embedded elliptical crack, the faces of which are subjected to arbitrary normal and shear tractions in [Vijayakumar and Atluri (1981)] are used.It was later successfully extended to BIE-FE alternating method for arbitrarily curved cracks for two dimensional problems in [Park and Atluri (1998)], and SGBEM-FE Alternating method for arbitrary three-dimensional non-planar embedded as well as surface flaws in [Nikishkov, Park and Atluri (2001), Han and Atluri (2002)]. The SGBEM-FE alternating method

can compute the stress intensity factors with low computational burden as well as high accuracy, and can model the fatigue growth of cracks without any re-meshing whatsoever. The reason why the series of works of Atluri and his coworkers, can compute stress intensity factors with high accuracy and low burden, is because the crack-singularities are modeled in the most efficient way—by complex variables, special functions, and by SGBEMs.

Boundary element methods (BEM) have distinct advantages over finite elements-for solving linear fracture mechanics problem. This is because BEM avoids using polynomial trial functions over the whole domain to approximate the singular fields. Discretization is only necessary at the boundary and crack surfaces. Moreover, the Symmetric Galerkin Boundary Element Methods (SGBEMs) have several advantages over traditional collocation BEMs, such as a symmetrical coefficient matrix of the system of equations, and no need to treat sharp corners specially, etc. Early derivations of SGBEMs involve regularization of hyper-singular integrals, see [Frangi and Novati (1996); Bonnet, Maier and Polizzotto (1998); Li, Mear and Xiao (1998); Frangi, Novati, Springhetti, Rovizzi(2002)]. Recently, a systematic procedure to develop weakly-singular symmetric Galerkin boundary integral equations was presented by [Han and Atluri (2003)]. The simple formulation derived in [Han and Atluri (2003)] involves only the non-hyper singular integral equations for tractions, based on the original work reported in [Okada, Rajiyah and Atluri (1988,1989), Atluri (2005)], and it was used to analyze cracked 3D solids with surface flaws in [Han and Atluri (2002)].

In this study, two-dimensional weakly-singular Symmetric Galerkin Boundary Elements (SGBEMs) are developed, following the work of [Han and Atluri (2003)]. Specifically, 2D SGBEMs are combined with some constraint conditions to model arbitrary shaped 2D cracks. Examples of embedded, edge, branching and intersecting cracks show high accuracy of computed stress intensity factors even with very coarse meshes. Non-collinear mixed-mode fatigue growth of arbitrary shaped cracks is also modeled. Minimal treatment is needed at each fatigue step—simply extending the cracks by adding an element to each crack tip, without the need for any re-meshing whatsoever.

However, because SGBEM always generates a system of equations with fully populated coefficient matrices, it is not suitable for modeling large-scale or complex structures. It is beneficial to model the global structure with finite elements, and model a local subdomain with SGBEM. This was realized by [Frangi and Novati (2003)] using weighted-residual weak-form, and by [Han and Atluri (2002)] using the alternating method. In this study, we develop a much simpler way to couple the SGBEM with traditional finite elements, or any other hybrid/mixed elements as by [Pian (1964); Atluri (1975); Dong and Atluri (2011a,b), Bishay and

Atluri(2012)], or special elements such as Trefftz Voronoi Cells in [Dong and Atluri (2012a,b,c)].The fundamental difference is that, a "Super Element" representing a local subdomain with arbitrary cracks within it, is developed, by rearranging the symmetric Galerkin boundary integral equations. The Super Element has a stiffness matrix and a force vector, which have physical meanings similar to those by traditional or special finite elements. Likewise, the stiffness matrix of the Super Element is also positive semi-definite and has exactly three rigid body modes. Therefore, Super Elements can thus be very simply implemented in any general-purpose finite element routine, using the simple assembly procedure. Super Elements are thus very suitable for analyzing large-scale structures and complex structures. Examples of cracked thin panels with stiffeners and composite patches are presented, showing the simplicity and efficiency of using SGBEM Super Elements to model cracked aircraft structures with stiffeners and composite patches.

The rest of this paper is organized as follows: in section 2, weakly-singular BIEs are developed for plane elasticity, while the corresponding kernel functions are presented in section 3; in section 4, a global SGBEM for 2D cracked structured is developed; in section 5, some discussion on cavities, edge cracks, branching and intersecting cracks is given; in section 6, some discussion on evaluating the stress intensity factors is given; in section 7, we present some numerical examples for the global SGBEM method; in section 8, we rearrange the weakly-singular BIEs to develop the Super Element; in section 9, numerical examples of the Super Elements are presented, with some emphasis on structures patched with composite laminates; in section 9, we complete this paper with some concluding remarks.

2 2D Weakly Singular BIEs for Plane Elasticity

Consider a linear elastic solid undergoing an infinitesimal elasto-static deformation. Cartesian coordinates ξ_i identify material particles in the solid; and Cartesian coordinates x_i identify the source point of the 2D Kelvin's solution, see Fig. 1. $\sigma_{ij}, \varepsilon_{ij}, u_i$ are Cartesian components of the stress tensor, strain tensor and displacement vector of the deformable solid, respectively. $\bar{f}_i$ are the components of the body force .We use $()_{,i}$ to denote differentiation with respect to ξ_i; and use $\frac{\partial}{\partial x_i}$ to denote differentiation with respect to x_i. The equations of linear and angular momentum balance, constitutive equations, and compatibility equations can be written as:

$$\sigma_{ij,i} + \bar{f}_j = 0 \quad \text{in } \Omega \tag{1}$$

$$\sigma_{ij} = \sigma_{ji} \quad \text{in } \Omega \tag{2}$$

$$\sigma_{ij} = E_{ijkl}\varepsilon_{kl} \quad \text{in } \Omega \tag{3}$$

$$\varepsilon_{ij} = \frac{1}{2}(u_{i,j} + u_{j,i}) \equiv u_{(i,j)} \quad \text{in } \Omega \tag{4}$$

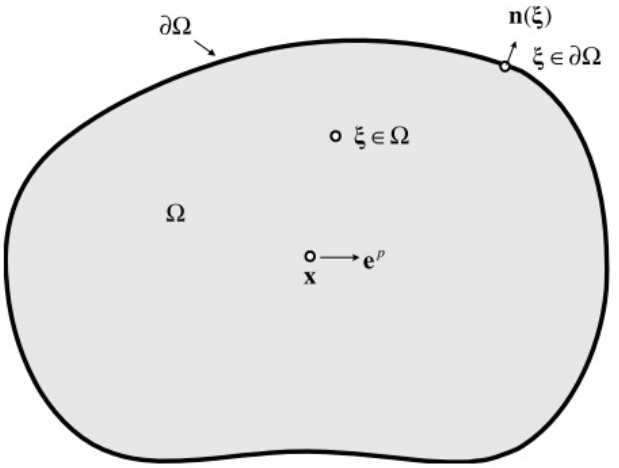

Figure 1: A solution domain with source point $\mathbf{x}$ and target point $\boldsymbol{\xi}$, taken from [Han and Atluri (2003)]

For isotropic plane elasticity,

$$E_{ijkl} = \mu\left(\frac{2\bar{v}}{1-2\bar{v}}\delta_{ij}\delta_{kl} + \delta_{ik}\delta_{jl} + \delta_{il}\delta_{jk}\right) \; i,j,k,l = 1,2$$
$$\bar{v} = \begin{cases} v & \text{for plane strain problems} \\ \frac{v}{1+v} & \text{for plane stress problems} \end{cases} \tag{5}$$

where μ, v are the shear modulus and Possion's ratio of the isotropic solid.
Equation (1)-(4) can be rewritten in terms of displacements as:

$$\left[E_{ijkl}u_{k,l}(\boldsymbol{\xi})\right]_{,i} + \bar{f}_j = 0 \tag{6}$$

Using $u_j^{*p}(\mathbf{x},\boldsymbol{\xi})$, the 2D Kelvin's solution corresponding to a unit force in direction $\mathbf{e_p}$ applied at source point $\mathbf{x}$, as the test function, we have:

$$\int_\Omega \left\{\left[E_{ijkl}u_{k,l}(\boldsymbol{\xi})\right]_{,i} + \bar{f}_j(\boldsymbol{\xi})\right\} u_j^{*p}(\mathbf{x},\boldsymbol{\xi})\, d\Omega_{\boldsymbol{\xi}} = 0 \tag{7}$$

wherethe 2D Kelvin's solution satisfies the equation:

$$\sigma_{ij,i}^{*p}(\mathbf{x},\boldsymbol{\xi}) = \left[E_{ijkl}u_{k,l}^{*p}(\mathbf{x},\boldsymbol{\xi})\right]_{,i} = -\delta_{jp}(\mathbf{x},\boldsymbol{\xi}) \tag{8}$$

where $\delta_{jp}(\mathbf{x},\boldsymbol{\xi}) = \delta_{jp}\delta(\mathbf{x},\boldsymbol{\xi})$ is a product of Kronecker delta and Dirac delta function.

Using the divergence theorem twice, we obtain the traditional displacement BIE:

$$\begin{aligned} &Cu_p(\mathbf{x}) = \int_{\partial\Omega} t_j(\boldsymbol{\xi}) u_j^{*p}(\mathbf{x},\boldsymbol{\xi}) dS_{\boldsymbol{\xi}} - \int_{\partial\Omega} u_j(\boldsymbol{\xi}) t_j^{*p}(\mathbf{x},\boldsymbol{\xi}) dS_{\boldsymbol{\xi}} \\ &+ \int_{\Omega} \bar{f}_j(\boldsymbol{\xi}) u_j^{*p}(\mathbf{x},\boldsymbol{\xi}) d\Omega_{\boldsymbol{\xi}} \end{aligned} \tag{9}$$

where

$$C = \begin{cases} 1 & \text{for } \mathbf{x} \in \Omega \\ \frac{1}{2} & \text{for } \mathbf{x} \in \partial\Omega \\ 0 & \text{else} \end{cases} \tag{10}$$

Similarly, using the gradient of the fundamental solution, namely $u_{j,k}^{*p}(\mathbf{x},\boldsymbol{\xi})$ as the test function, we have:

$$\int_{\Omega} \left\{ \left[E_{ijmn} u_{m,n}(\boldsymbol{\xi}) \right]_{,i} + \bar{f}_j(\boldsymbol{\xi}) \right\} u_{j,k}^{p}(\mathbf{x},\boldsymbol{\xi}) \, d\Omega_{\boldsymbol{\xi}} = 0 \tag{11}$$

Using divergence theorem three times, we obtain the BIE for $u_{p,k}(\mathbf{x})$:

$$\begin{aligned} &-Cu_{p,k}(\mathbf{x}) = \int_{\partial\Omega} t_j(\xi) u_{j,k}^{*p}(\mathbf{x},\boldsymbol{\xi}) dS_{\boldsymbol{\xi}} \\ &+ \int_{\partial\Omega} n_n(\boldsymbol{\xi}) u_{m,k}(\boldsymbol{\xi}) \sigma_{nm}^{*p}(\mathbf{x},\boldsymbol{\xi}) dS_{\boldsymbol{\xi}} - \int_{\partial\Omega} n_k(\boldsymbol{\xi}) u_{m,n}(\boldsymbol{\xi}) \sigma_{nm}^{*p}(\mathbf{x},\boldsymbol{\xi}) dS_{\boldsymbol{\xi}} \\ &+ \int_{\Omega} \bar{f}_j(\boldsymbol{\xi}) u_{j,k}^{*p}(\mathbf{x},\boldsymbol{\xi}) d\Omega_{\boldsymbol{\xi}} \end{aligned} \tag{12}$$

Eq. (12) was originally given in [Okada, Rajiyah, and Atluri (1988,1989)], which is only strongly-singular, as opposed to the hyper-singular BIE obtained by directly differentiating Eq. (9). For 2D problems, we define a tangential differential operator D:

$$\begin{aligned} D(\boldsymbol{\xi}) &= n_r(\boldsymbol{\xi}) e_{rs} \frac{\partial}{\partial \xi_s} \\ D(\mathbf{x}) &= n_r(\mathbf{x}) e_{rs} \frac{\partial}{\partial x_s} \end{aligned} \tag{13}$$

where the 2D Levi-Civita symbol e_{rs} is an analogy to the 3D Levi-Civita symbol:

$$e_{11} = e_{22} = 0; \; e_{12} = 1; \; e_{21} = -1 \tag{14}$$

e_{rs} has the following properties:

$$\begin{aligned} e_{rs} e_{nk} &= \delta_{rn}\delta_{sk} - \delta_{rk}\delta_{sn} \\ e_{rs} e_{rt} &= \delta_{st} \end{aligned} \tag{15}$$

Eq. (12) is thereafter rewritten as:

$$\begin{aligned} &-Cu_{p,k}(\mathbf{x}) = \int_{\partial\Omega} t_j(\xi) u_{j,k}^{*p}(\mathbf{x},\boldsymbol{\xi}) dS_{\boldsymbol{\xi}} + \int_{\partial\Omega} D(\boldsymbol{\xi}) u_m(\boldsymbol{\xi}) e_{nk} \sigma_{nm}^{*p}(\mathbf{x},\boldsymbol{\xi}) dS_{\boldsymbol{\xi}} \\ &+ \int_{\Omega} \bar{f}_j(\boldsymbol{\xi}) u_{j,k}^{*p}(\mathbf{x},\boldsymbol{\xi}) d\Omega_{\boldsymbol{\xi}} \end{aligned} \tag{16}$$

Pre-multiplying(16)by E_{abpk}, and using the inherent property of the Kelvin's solution $u_j^{*p} = u_p^{*j}$, we obtain a BIE for the stress tensor of 2D plane elasticity:

$$\begin{aligned} &-C\sigma_{ab}(\mathbf{x}) = \int_{\partial\Omega} t_p(\xi)\sigma_{ab}^{*p}(\mathbf{x},\boldsymbol{\xi})dS_{\boldsymbol{\xi}} + \int_{\partial\Omega} D(\boldsymbol{\xi})u_q(\boldsymbol{\xi})\Sigma_{abq}^{*}(\mathbf{x},\boldsymbol{\xi})dS_{\boldsymbol{\xi}} \\ &+ \int_{\Omega} \bar{f}_p(\boldsymbol{\xi})\sigma_{ab}^{*p}(\mathbf{x},\boldsymbol{\xi})d\Omega_{\boldsymbol{\xi}} \end{aligned} \tag{17}$$

where

$$\Sigma_{abq}^{*}(\mathbf{x},\boldsymbol{\xi}) = E_{abkl}e_{nl}\sigma_{nq}^{*k}(\mathbf{x},\boldsymbol{\xi}) \tag{18}$$

And the traction BIE can be obtained by contracting (17) with $n_a(\mathbf{x})$:

$$\begin{aligned} &-Ct_b(\mathbf{x}) = \int_{\partial\Omega} t_p(\boldsymbol{\xi})n_a(\mathbf{x})\sigma_{ab}^{*p}(\mathbf{x},\boldsymbol{\xi})dS_{\boldsymbol{\xi}} + \int_{\partial\Omega} D(\boldsymbol{\xi})u_q(\xi)n_a(\mathbf{x})\Sigma_{abq}^{*}(\mathbf{x},\boldsymbol{\xi})dS_{\boldsymbol{\xi}} \\ &+ \int_{\Omega} \bar{f}_p(\boldsymbol{\xi})n_a(\mathbf{x})\sigma_{ab}^{*p}(\mathbf{x},\boldsymbol{\xi})d\Omega_{\boldsymbol{\xi}} \end{aligned} \tag{19}$$

The above traction BIE in Eq (19) is NOT hyper-singular. We would like to point out that, the 2D Levi-Civita symbol e_{rs} is only a speical case of the 3D Levi-Civita symbol e_{rst}. Consider $\mathbf{f}$ and $\mathbf{g}$ as two 3D vectors which stay in the $x_1 - x_2$ plane, we have $\mathbf{f} \times \mathbf{g} = e_{ij}f_i g_j \mathbf{e}_3$, and $\nabla \times \mathbf{f} = e_{ij}f_{j.i}\mathbf{e}_3$. Since the direction is prescribed to be $\mathbf{e}_3$, we simply drop $\mathbf{e_3}$, and denote the cross product of two 2D vectors $\mathbf{f}$ and $\mathbf{g}$ as $e_{ij}f_i g_j$, and the curl of $\mathbf{f}$ as $e_{ij}f_{j.i}$.

According to Helmholtz theorem, any vector field (and of course, second order tensor, third order tensor, etc.) can be decomposed into the summation of an irrotational field and a solenoidal field. Therefore, $\sigma_{ij}^{*p}(\mathbf{x},\boldsymbol{\xi})$ can be decomposed as:

$$\sigma_{ij}^{*p}(\mathbf{x},\boldsymbol{\xi}) = -\phi_{ij}^{*p}(\mathbf{x},\boldsymbol{\xi}) + \psi_{ij}^{*p}(\mathbf{x},\boldsymbol{\xi}) \tag{20}$$

where

$$\begin{aligned} \phi_{ij}^{*p}(\mathbf{x},\boldsymbol{\xi}) &= M_{j,i}^{*p}(\mathbf{x},\boldsymbol{\xi}) \\ \psi_{ij}^{*p}(\mathbf{x},\boldsymbol{\xi}) &= e_{is}G_{j,s}^{*p}(\mathbf{x},\boldsymbol{\xi}) \end{aligned} \tag{21}$$

And $\Sigma_{ijq}^{*}(\mathbf{x},\boldsymbol{\xi})$ can be decomposed as:

$$\Sigma_{ijq}^{*}(\mathbf{x},\boldsymbol{\xi}) = -\Lambda_{ijq}^{*}(\mathbf{x},\boldsymbol{\xi}) + K_{ijq}^{*}(\mathbf{x},\boldsymbol{\xi}) \tag{22}$$

where

$$\begin{aligned} \Lambda_{ijq}^{*}(\mathbf{x},\boldsymbol{\xi}) &= N_{jq,i}^{*}(\mathbf{x},\boldsymbol{\xi}) \\ K_{ijq}^{*}(\mathbf{x},\boldsymbol{\xi}) &= e_{is}H_{jq,s}^{*}(\mathbf{x},\boldsymbol{\xi}) \end{aligned} \tag{23}$$

The decomposition of $\sigma_{ij}^{*p}(\mathbf{x},\boldsymbol{\xi})$ and $\Sigma_{ijq}^{*}(\mathbf{x},\boldsymbol{\xi})$ is worked out in detail, and will be presented in section 3. As opposed to 3D problems, $\Sigma_{ijq}^{*}(\mathbf{x},\boldsymbol{\xi})$ is itself solenoidal for 2D problems. Therefore $\Lambda_{ijq}^{*}(\mathbf{x},\boldsymbol{\xi})$ vanishes for 2D problems.

As shown in [Han and Atluri (2003)], decomposed kernel functions can be used to regularize the displacement and traction BIEs. Using the same approach, we consider the traction BIE (19) and a test function $w_b(\mathbf{x})$, and write down the Petrov-Galerkin weak-form:

$$\begin{aligned}
&-\tfrac{1}{2}\textstyle\int_{\partial\Omega} w_b(\mathbf{x})t_b(\mathbf{x})dS_{\mathbf{x}} = \int_{\partial\Omega} w_b(\mathbf{x})dS_{\mathbf{x}} \int_{\partial\Omega} t_q(\boldsymbol{\xi})n_a(\mathbf{x})\sigma_{ab}^{*q}(\mathbf{x},\boldsymbol{\xi})\,dS_{\boldsymbol{\xi}} \\
&+\textstyle\int_{\partial\Omega} w_b(\mathbf{x})dS_{\mathbf{x}} \int_{\partial\Omega} D(\boldsymbol{\xi})u_q(\boldsymbol{\xi})n_a(\mathbf{x})\Sigma_{abq}^{*}(\mathbf{x},\boldsymbol{\xi})dS_{\boldsymbol{\xi}} \\
&+\textstyle\int_{\partial\Omega} w_b(\mathbf{x})dS_{\mathbf{x}} \int_{\Omega} \bar{f}_q(\boldsymbol{\xi})n_a(\mathbf{x})\sigma_{ab}^{*q}(\mathbf{x},\boldsymbol{\xi})\,d\Omega_{\boldsymbol{\xi}}
\end{aligned} \tag{24}$$

Substituting (20)-(23) into (24), we have:

$$\begin{aligned}
&-\tfrac{1}{2}\textstyle\int_{\partial\Omega} w_b(\mathbf{x})t_b(\mathbf{x})dS_{\mathbf{x}} \\
&=\textstyle\int_{\partial\Omega} w_b(\mathbf{x})dS_{\mathbf{x}} \int_{\partial\Omega} t_q(\boldsymbol{\xi})n_a(\mathbf{x})e_{as}G_{b,s}^{*q}(\mathbf{x},\boldsymbol{\xi})\,dS_{\boldsymbol{\xi}} \\
&-\textstyle\int_{\partial\Omega} w_b(\mathbf{x})dS_{\mathbf{x}} \int_{\partial\Omega} t_q(\boldsymbol{\xi})n_a(\mathbf{x})\phi_{ab}^{*q}(\mathbf{x},\boldsymbol{\xi})\,dS_{\boldsymbol{\xi}} \\
&+\textstyle\int_{\partial\Omega} w_b(\mathbf{x})dS_{\mathbf{x}} \int_{\partial\Omega} D(\boldsymbol{\xi})u_q(\boldsymbol{\xi})n_a(\mathbf{x})e_{as}H_{bq,s}^{*}(\mathbf{x},\boldsymbol{\xi})dS_{\boldsymbol{\xi}} \\
&+\textstyle\int_{\partial\Omega} w_b(\mathbf{x})dS_{\mathbf{x}} \int_{\Omega} \bar{f}_q(\boldsymbol{\xi})n_a(\mathbf{x})\sigma_{ab}^{*q}(\mathbf{x},\boldsymbol{\xi})\,d\Omega_{\boldsymbol{\xi}}
\end{aligned} \tag{25}$$

For any function $L(\mathbf{x}-\boldsymbol{\xi})$ which depends only on the relative location of $\mathbf{x},\boldsymbol{\xi}$, such as $u_b^{*q}(\mathbf{x},\boldsymbol{\xi}), G_b^{*q}(\mathbf{x},\boldsymbol{\xi}), M_b^{*q}(\mathbf{x},\boldsymbol{\xi}), H_{bq}^{*}(\mathbf{x},\boldsymbol{\xi})$, we have:

$$\frac{\partial L(\mathbf{x}-\boldsymbol{\xi})}{\partial x_i} = -\frac{\partial L(\mathbf{x}-\boldsymbol{\xi})}{\partial \xi_i} = -L_{,i}(\mathbf{x}-\boldsymbol{\xi}) \tag{26}$$

Therefore, (25) can be rewritten as:

$$\begin{aligned}
&-\tfrac{1}{2}\textstyle\int_{\partial\Omega} w_b(\mathbf{x})t_b(\mathbf{x})dS_{\mathbf{x}} \\
&=-\textstyle\int_{\partial\Omega} n_a(\mathbf{x})e_{as}w_b(\mathbf{x})dS_{\mathbf{x}} \frac{\partial}{\partial x_s}\int_{\partial\Omega} t_q(\boldsymbol{\xi})G_b^{*q}(\mathbf{x},\boldsymbol{\xi})\,dS_{\boldsymbol{\xi}} \\
&-\textstyle\int_{\partial\Omega} w_b(\mathbf{x})dS_{\mathbf{x}} \int_{\partial\Omega} n_a(\mathbf{x})t_q(\boldsymbol{\xi})\phi_{ab}^{*q}(\mathbf{x},\boldsymbol{\xi})\,dS_{\boldsymbol{\xi}} \\
&-\textstyle\int_{\partial\Omega} n_a(\mathbf{x})e_{as}w_b(\mathbf{x})dS_{\mathbf{x}} \frac{\partial}{\partial x_s}\int_{\partial\Omega} D(\boldsymbol{\xi})u_q(\boldsymbol{\xi})H_{bq}^{*}(\mathbf{x},\boldsymbol{\xi})dS_{\boldsymbol{\xi}} \\
&+\textstyle\int_{\partial\Omega} w_b(\mathbf{x})dS_{\mathbf{x}} \int_{\Omega} \bar{f}_q(\boldsymbol{\xi})n_a(\mathbf{x})\sigma_{ab}^{*q}(\mathbf{x},\boldsymbol{\xi})\,d\Omega_{\boldsymbol{\xi}}
\end{aligned} \tag{27}$$

Using Green's theorem, we have:

$$\begin{aligned}
&-\tfrac{1}{2}\textstyle\int_{\partial\Omega} w_b(\mathbf{x})t_b(\mathbf{x})dS_{\mathbf{x}} \\
&=\textstyle\int_{\partial\Omega} n_a(\mathbf{x})e_{as}\frac{\partial w_b(\mathbf{x})}{\partial x_s}dS_{\mathbf{x}} \int_{\partial\Omega} t_q(\boldsymbol{\xi})G_b^{*q}(\mathbf{x},\boldsymbol{\xi})\,dS_{\boldsymbol{\xi}} \\
&-\textstyle\int_{\partial\Omega} w_b(\mathbf{x})dS_{\mathbf{x}} \int_{\partial\Omega} n_a(\mathbf{x})t_q(\boldsymbol{\xi})\phi_{ab}^{*q}(\mathbf{x},\boldsymbol{\xi})\,dS_{\boldsymbol{\xi}} \\
&+\textstyle\int_{\partial\Omega} n_a(\mathbf{x})e_{as}\frac{\partial w_b(\mathbf{x})}{\partial x_s}dS_{\mathbf{x}} \int_{\partial\Omega} D(\boldsymbol{\xi})u_q(\boldsymbol{\xi})H_{bq}^{*}(\mathbf{x},\boldsymbol{\xi})dS_{\boldsymbol{\xi}} \\
&+\textstyle\int_{\partial\Omega} w_b(\mathbf{x})dS_{\mathbf{x}} \int_{\Omega} \bar{f}_q(\boldsymbol{\xi})n_a(\mathbf{x})\sigma_{ab}^{*q}(\mathbf{x},\boldsymbol{\xi})\,d\Omega_{\boldsymbol{\xi}}
\end{aligned} \tag{28}$$

which is identical to:

$$\begin{aligned}
&-\tfrac{1}{2}\int_{\partial\Omega} w_b(\mathbf{x})t_b(\mathbf{x})dS_{\mathbf{x}} \\
&=\int_{\partial\Omega} D(\mathbf{x})w_b(\mathbf{x})dS_{\mathbf{x}}\int_{\partial\Omega} t_q(\boldsymbol{\xi})G_b^{*q}(\mathbf{x},\boldsymbol{\xi})\,dS_{\boldsymbol{\xi}} \\
&-\int_{\partial\Omega} w_b(\mathbf{x})dS_{\mathbf{x}}\int_{\partial\Omega} n_a(\mathbf{x})t_q(\boldsymbol{\xi})\phi_{ab}^{*q}(\mathbf{x},\boldsymbol{\xi})\,dS_{\boldsymbol{\xi}} \\
&+\int_{\partial\Omega} D(\mathbf{x})w_b(\mathbf{x})dS_{\mathbf{x}}\int_{\partial\Omega} D(\boldsymbol{\xi})u_q(\boldsymbol{\xi})H_{bq}^{*}(\mathbf{x},\boldsymbol{\xi})dS_{\boldsymbol{\xi}} \\
&+\int_{\partial\Omega} w_b(\mathbf{x})dS_{\mathbf{x}}\int_{\Omega}\bar{f}_q(\boldsymbol{\xi})n_a(\mathbf{x})\sigma_{ab}^{*q}(\mathbf{x},\boldsymbol{\xi})\,d\Omega_{\boldsymbol{\xi}}
\end{aligned} \tag{29}$$

Similarly, using the displacement BIE in (9), and a test function $v_b(\mathbf{x})$, we write down the Petrov-Galerkin weak-form:

$$\begin{aligned}
&\tfrac{1}{2}\int_{\partial\Omega} v_p(\mathbf{x})u_p(\mathbf{x})dS_x=\int_{\partial\Omega} v_p(\mathbf{x})dS_x\int_{\partial\Omega} t_j(\boldsymbol{\xi})u_j^{*p}(\mathbf{x},\boldsymbol{\xi})dS_{\boldsymbol{\xi}} \\
&-\int_{\partial\Omega} v_p(\mathbf{x})dS_x\int_{\partial\Omega} n_i(\boldsymbol{\xi})u_j(\boldsymbol{\xi})\sigma_{ij}^{*p}(\mathbf{x},\boldsymbol{\xi})\,dS_{\boldsymbol{\xi}} \\
&+\int_{\partial\Omega} v_p(\mathbf{x})dS_x\int_{\partial\Omega}\bar{f}_j(\boldsymbol{\xi})u_j^{*p}(\mathbf{x},\boldsymbol{\xi})d\Omega_{\boldsymbol{\xi}}
\end{aligned} \tag{30}$$

Substituting (20)-(23) into (30), we have:

$$\begin{aligned}
&\tfrac{1}{2}\int_{\partial\Omega} v_p(\mathbf{x})u_p(\mathbf{x})dS_x=\int_{\partial\Omega} v_p(\mathbf{x})dS_x\int_{\partial\Omega} t_j(\boldsymbol{\xi})u_j^{*p}(\mathbf{x},\boldsymbol{\xi})dS_{\boldsymbol{\xi}} \\
&-\int_{\partial\Omega} v_p(\mathbf{x})dS_x\int_{\partial\Omega} n_i(\boldsymbol{\xi})u_j(\boldsymbol{\xi})e_{is}G_{j,s}^{*p}(\mathbf{x},\boldsymbol{\xi})\,dS_{\boldsymbol{\xi}} \\
&+\int_{\partial\Omega} v_p(\mathbf{x})dS_x\int_{\partial\Omega} n_i(\boldsymbol{\xi})u_j(\boldsymbol{\xi})\phi_{ij}^{*p}(\mathbf{x},\boldsymbol{\xi})\,dS_{\boldsymbol{\xi}} \\
&+\int_{\partial\Omega} v_p(\mathbf{x})dS_x\int_{\partial\Omega}\bar{f}_j(\boldsymbol{\xi})u_j^{*p}(\mathbf{x},\boldsymbol{\xi})d\Omega_{\boldsymbol{\xi}}
\end{aligned} \tag{31}$$

Using Green's theorem, we have:

$$\begin{aligned}
&\tfrac{1}{2}\int_{\partial\Omega} v_p(\mathbf{x})u_p(\mathbf{x})dS_x=\int_{\partial\Omega} v_p(\mathbf{x})dS_x\int_{\partial\Omega} t_j(\boldsymbol{\xi})u_j^{*p}(\mathbf{x},\boldsymbol{\xi})dS_{\boldsymbol{\xi}} \\
&+\int_{\partial\Omega} v_p(\mathbf{x})dS_x\int_{\partial\Omega} n_i(\boldsymbol{\xi})e_{is}u_{j,s}(\boldsymbol{\xi})G_j^{*p}(\mathbf{x},\boldsymbol{\xi})\,dS_{\boldsymbol{\xi}} \\
&+\int_{\partial\Omega} v_p(\mathbf{x})dS_x\int_{\partial\Omega} n_i(\boldsymbol{\xi})u_j(\boldsymbol{\xi})\phi_{ij}^{*p}(\mathbf{x},\boldsymbol{\xi})\,dS_{\boldsymbol{\xi}} \\
&+\int_{\partial\Omega} v_p(\mathbf{x})dS_x\int_{\partial\Omega}\bar{f}_j(\boldsymbol{\xi})u_j^{*p}(\mathbf{x},\boldsymbol{\xi})d\Omega_{\boldsymbol{\xi}}
\end{aligned} \tag{32}$$

which is identical to:

$$\begin{aligned}
&\tfrac{1}{2}\int_{\partial\Omega} v_p(\mathbf{x})u_p(\mathbf{x})dS_x=\int_{\partial\Omega} v_p(\mathbf{x})dS_x\int_{\partial\Omega} t_j(\boldsymbol{\xi})u_j^{*p}(\mathbf{x},\boldsymbol{\xi})dS_{\boldsymbol{\xi}} \\
&+\int_{\partial\Omega} v_p(\mathbf{x})dS_x\int_{\partial\Omega} D(\boldsymbol{\xi})u_j(\boldsymbol{\xi})G_j^{*p}(\mathbf{x},\boldsymbol{\xi})\,dS_{\boldsymbol{\xi}} \\
&+\int_{\partial\Omega} v_p(\mathbf{x})dS_x\int_{\partial\Omega} n_i(\boldsymbol{\xi})u_j(\boldsymbol{\xi})\phi_{ij}^{*p}(\mathbf{x},\boldsymbol{\xi})\,dS_{\boldsymbol{\xi}} \\
&+\int_{\partial\Omega} v_p(\mathbf{x})dS_x\int_{\partial\Omega}\bar{f}_j(\boldsymbol{\xi})u_j^{*p}(\mathbf{x},\boldsymbol{\xi})d\Omega_{\boldsymbol{\xi}}
\end{aligned} \tag{33}$$

Eqs.(29)-(33) developed here are only weakly singular, because as will be shown in section 3, kernels $u_b^{*q}(\mathbf{x},\boldsymbol{\xi})$, $G_b^{*q}(\mathbf{x},\boldsymbol{\xi})$, $H_{bq}^{*}(\mathbf{x},\boldsymbol{\xi})$, $n_i(\boldsymbol{\xi})\phi_{ij}^{*p}(\mathbf{x},\boldsymbol{\xi})$, $n_i(\mathbf{x})\phi_{ij}^{*p}(\mathbf{x},\boldsymbol{\xi})$ are all weakly-singular. Therefore, the implementation of (29)-(33) for SGBEM can be easily carried out.

It should be noted that,the BIEs developed here for 2D problems, may look slightly different from those original ones in [Han and Atluri(2003)]. However, they have

no difference essentially. The 2D Levi-Civita symbol is a special case of the 3D Levi-Civita symbol. And the Green theorem as used in this derivation is only a special case of the 3D Strokes theorem used in [Han and Atluri(2003)]. If one carefully disinguish the in-plane and out-of-plane components of every tensor in [Han and Atluri (2003)], all the BIEs and corresponding kernels in their study reduce to the current ones.

3 Decomposition of the 2D Kelvin's Solution

The 2D Kelvin's solution, which corresponds to a concentrated load in an infinite plane medium, can be expressed in terms of the Boussinesq-Galerkin general solution:

$$u_i^{*p} = b_{i,kk}^{*p} - \frac{1}{2(1-\bar{\nu})} b_{k,ki}^{*p} \tag{34}$$

where the Boussinesq-Galerkin potential is:

$$\begin{aligned} &b_i^{*p} = (1-\bar{\nu})\delta_{ip} F^* \\ &F^* = \tfrac{-r^2 \ln r}{8\pi\mu(1-\bar{\nu})} \end{aligned} \tag{35}$$

We have:

$$u_i^{*p} = (1-\bar{\nu})\delta_{pi} F_{,kk}^* - \frac{1}{2} F_{,pi}^* \tag{36}$$

$$\begin{aligned} &\sigma_{ij}^{*p} = \mu \left[(1-\bar{\nu})\delta_{pi} F_{,kkj}^* + \bar{\nu}\delta_{ij} F_{,pkk}^* - F_{,pij}^* \right] \\ &+\mu(1-\bar{\nu})\delta_{pj} F_{,kki}^* \end{aligned} \tag{37}$$

$$\begin{aligned} &\sigma_{ij,i}^{*p} = \mu \left[(1-\bar{\nu})\delta_{pi} F_{,kkji}^* + \bar{\nu}\delta_{ij} F_{,pkki}^* - F_{,piji}^* \right] \\ &+\mu(1-\bar{\nu})\delta_{pj} F_{,kkii}^* \\ &= \mu(1-\bar{\nu})\delta_{pj} F_{,kkii}^* \end{aligned} \tag{38}$$

Therefore, the irrotational part of σ_{ij}^{*p} can be easily found as:

$$\begin{aligned} &\phi_{ij}^{*p} = -\mu(1-\bar{\nu})\delta_{pj} F_{,kki}^* = M_{j,i}^{*p} \\ &M_j^{*p} = -\mu(1-\bar{\nu})\delta_{pj} F_{,kk}^* \end{aligned} \tag{39}$$

And the solenoidal part is:

$$\begin{aligned} &\Psi_{ij}^{*p} = \sigma_{ij}^{*p} + \phi_{ij}^{*p} = \mu \left[(1-\bar{\nu})\delta_{pi} F_{,kkj}^* + \bar{\nu}\delta_{ij} F_{,pkk}^* - F_{,pij}^* \right] \\ &= e_{is}\mu \left[(1-\bar{\nu}) e_{pj} F_{,kk}^* - e_{kj} F_{pk}^* \right]_{,s} = e_{is} G_{j,s}^{*p} \\ &G_j^{*p} = \mu \left[(1-\bar{\nu}) e_{pj} F_{,kk}^* - e_{kj} F_{pk}^* \right] \end{aligned} \tag{40}$$

After some manipulation, we can see that:

$$\begin{aligned}
&\Sigma^*_{ijq} = E_{ijkl}e_{nl}\sigma^{*k}_{nq} \\
&= \mu^2\left(\tfrac{2\bar{\nu}}{1-2\bar{\nu}}\delta_{ij}\delta_{kl}+\delta_{ik}\delta_{jl}+\delta_{il}\delta_{jk}\right)e_{nl} \\
&\left[(1-\bar{\nu})\left(\delta_{kn}F^*_{,bbq}+\delta_{kq}F^*_{,bbn}\right)+\bar{\nu}\delta_{nq}F^*_{,bbk}-F^*_{,knq}\right] \\
&= 2\mu^2\left(e_{in}F_{,jqn}-e_{in}\delta_{jq}F_{,bbn}\right) \\
&= e_{in}2\mu^2\left(F_{,jq}-\delta_{jq}F_{,bb}\right)_{,n} \\
&= e_{in}H^*_{jq,n}
\end{aligned} \tag{41}$$

where,

$$H^*_{jq} = 2\mu^2\left(F_{,jq}-\delta_{jq}F_{,bb}\right) \tag{42}$$

From (41), we see that Σ^*_{ijq} itself is solenoidal.
Using the definition of F^*, we write down the kernel functions for 2D problems:

$$\begin{aligned}
&u^{*p}_j = \tfrac{1}{8\pi\mu(1-\bar{\nu})}\left[-(3-4\bar{\nu})\ln r\delta_{jp}+r_{,j}r_{,p}\right] \\
&u^{*p}_{j,k} = \tfrac{1}{8\pi\mu(1-\bar{\nu})r}\left[-(3-4\bar{\nu})r_{,k}\delta_{jp}-2r_{,j}r_{,p}r_{,k}+\delta_{pk}r_{,j}+\delta_{jk}r_{,p}\right] \\
&G^{*p}_j = \tfrac{1}{8\pi(1-\bar{\nu})}\left[e_{pj}\left[(4\bar{\nu}-3)+2(2\bar{\nu}-1)\ln r\right]+2e_{kj}r_{,k}r_{,p}\right] \\
&\Psi^{*p}_{ij} = e_{is}G^{*p}_{j,s} = \tfrac{1}{4\pi(1-\bar{\nu})r}\left[(1-2\bar{\nu})(\delta_{ij}r_{,p}-\delta_{ip}r_{,j})-2r_{,i}r_{,j}r_{,p}+\delta_{jp}r_{,i}\right] \\
&M^{*p}_j = \tfrac{1}{2\pi}\left(1+\ln r\right)\delta_{pj} \\
&\phi^{*p}_{ij} = M^{*p}_{j,i} = \tfrac{1}{2\pi r}\delta_{pj}r_{,i} \\
&\sigma^{*p}_{ij} = -\phi^{*p}_{ij}+\Psi^{*p}_{ij} = \tfrac{1}{4\pi(1-\bar{\nu})r}\left[(1-2\bar{\nu})(\delta_{ij}r_{,p}-\delta_{ip}r_{,j}-\delta_{jp}r_{,i})-2r_{,i}r_{,j}r_{,p}\right] \\
&H^*_{jq} = \tfrac{\mu}{4\pi(1-\bar{\nu})}\left[\delta_{qj}\left(3+2\ln r\right)-2r_{,j}r_{,q}\right] \\
&\Sigma^*_{ijq} = e_{in}H^*_{jq,n} = \tfrac{\mu}{2\pi(1-\bar{\nu})r}e_{in}\left[2r_{,j}r_{,q}r_{,n}+\delta_{qj}r_{,n}-\delta_{qn}r_{,j}-\delta_{jn}r_{,q}\right]
\end{aligned} \tag{43}$$

It should be noted that, in the formulae of potentials $G^{*p}_j, M^{*p}_j, \Sigma^*_{ijq}$ as shown in (43), constant terms can be eliminated for simplicity, which have no influence on their gradient or curl fields.

4 Global SGBEM for 2D Plane Elasticity of an Isotropic Body With Arbitrary Shaped Cracks & Cavities

Consider an isotropicsolid body Ω undergoing infinitesimal elasto-static deformations, the whole boundary of which is defined by a number of contours and lines. One contour S_0 defines the outer boundary, and the other contours $S_i, i = 1,2...$ are the boundaries of cavities contained in the solid body. The lines $L_i, i = 1,2...$represent the cracks, each of which can be divided to L^+_i, L^-_i , the two opposite surfaces of each crack. The boundary $\partial\Omega$ is a summation of all the contours

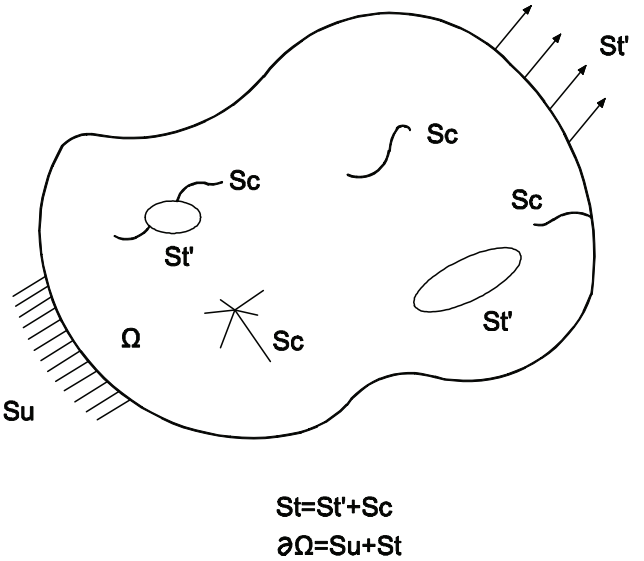

Figure 2: A defective solid with arbitrary cavities and cracks

and lines: $\partial\Omega = \sum_i S_i + \sum_i L_i$. Based on the types of boundary conditions, the whole boundary $\partial\Omega$ can also be divided to:

S_u, the part of $\sum_i S_i$ where displacements are prescribed,

S'_t, the part of $\sum_i S_i$ where tractions are prescribed,

S_c, the crack surface defined by smooth lines.

S_c^+, S_c^- are the two opposite surfaces of the crack , the displacements and tractions on which are denoted as $u_i^+, u_i^-, t_i^+, t_i^-$ respectively.

Boundary conditions are:

$$\begin{aligned} &u_i = \bar{u}_i \text{ at } S_u \\ &t_i = \bar{t}_i \text{ at } S'_t \\ &t_i^+ = -t_i^- = \bar{t}_i \text{ at } S_c \end{aligned} \tag{44}$$

We consider the crack surface to be part of the entire traction-prescribed boundary S_t, and we have $S_t = S'_t + S_c$. At S'_t, the tractions t_i are prescribed to be $\bar{t}_i$, and u_i are to be determined. At the crack surfaceS_c,the tractions t_i^+ are prescribed to be $\bar{t}_i$, t_i^- are prescribed to be $-\bar{t}_i$, and $\Delta u_i = u_i^+ - u_i^-$ are to be determined. Without introducing any ambiguity, we still use u_i to denote the undetermined displacement discontinuity at the crack surface, instead of Δu_i. The displacement and traction

BIEs developed in the last section can still be directly used, where u_i and t_i should be interpreted as Δu_i and $\bar{t}_i$ respectively at the crack surface.

For SGBRM, test function v_p, w_p for displacement BIE is assumed as:

$$v_p = \begin{cases} \delta t_p \text{ at } S_u \\ 0 \text{ at } S_t \end{cases}$$
$$w_p = \begin{cases} 0 \text{ at } S_u \\ \delta u_p \text{ at } S_t \end{cases} \tag{45}$$

Displacements and tractions are assumed in terms of nodal shape functions:

$$\begin{aligned} u_i &= N^q \bar{u}_i^q \text{ at } S_u \\ t_i &= M^q t_i^q \text{ at } S_u \\ u_i &= N^q u_i^q \text{ at } S_t \\ t_i &= M^q \bar{t}_i^q \text{ at } S_t \end{aligned} \tag{46}$$

where repeated indices indicate a summation.

Discretized BIEs are therefore expressed as:

$$\begin{aligned} &-\tfrac{1}{2}\delta t_p^n \textstyle\int_{S_u} M^n(\mathbf{x}) N^m(\mathbf{x}) dS_x \bar{u}_p^m \\ &+\delta t_p^n \textstyle\int_{S_u} M^n(\mathbf{x}) dS_x \int_{S_t} u_j^{*p}(\mathbf{x},\boldsymbol{\xi}) M^m(\boldsymbol{\xi}) dS_{\boldsymbol{\xi}} \bar{t}_j^m \\ &+\delta t_p^n \textstyle\int_{S_u} M^n(\mathbf{x}) dS_x \int_{S_u} G_j^{*p}(\mathbf{x},\boldsymbol{\xi}) D(\boldsymbol{\xi}) N^m(\xi) dS_{\boldsymbol{\xi}} \bar{u}_j^m \\ &+\delta t_p^n \textstyle\int_{S_u} M^n(\mathbf{x}) dS_x \int_{S_u} n_i(\boldsymbol{\xi}) \phi_{ij}^{*p}(\mathbf{x},\boldsymbol{\xi}) N^m(\boldsymbol{\xi}) dS_{\boldsymbol{\xi}} \bar{u}_j^m \\ &= -\delta t_p^n \textstyle\int_{S_u} M^n(\mathbf{x}) dS_x \int_{S_u} u_j^{*p}(\mathbf{x},\boldsymbol{\xi}) M^m(\boldsymbol{\xi}) dS_{\boldsymbol{\xi}} t_j^m \\ &-\delta t_p^n \textstyle\int_{S_u} M^n(\mathbf{x}) dS_x \int_{S_t} G_j^{*p}(\mathbf{x},\boldsymbol{\xi}) D(\boldsymbol{\xi}) N^m(\xi) dS_{\boldsymbol{\xi}} u_j^m \\ &-\delta t_p^n \textstyle\int_{S_u} M^n(\mathbf{x}) dS_x \int_{S_t} n_i(\boldsymbol{\xi}) \phi_{ij}^{*p}(\mathbf{x},\boldsymbol{\xi}) N^m(\boldsymbol{\xi}) dS_{\boldsymbol{\xi}} u_j^m \end{aligned} \tag{47}$$

$$\begin{aligned} &\tfrac{1}{2}\delta u_b^n \textstyle\int_{S_t} N^n(\mathbf{x}) M^m(\mathbf{x}) dS_{\mathbf{x}} \bar{t}_b^m \\ &+\delta u_b^n \textstyle\int_{S_t} D(\mathbf{x}) N^n(\mathbf{x}) dS_{\mathbf{x}} \int_{S_t} G_b^{*q}(\mathbf{x},\boldsymbol{\xi}) M^m(\xi) dS_{\boldsymbol{\xi}} \bar{t}_q^m \\ &-\delta u_b^n \textstyle\int_{S_t} N^n(\mathbf{x}) dS_{\mathbf{x}} \int_{S_t} n_a(\mathbf{x}) \phi_{ab}^{*q}(\mathbf{x},\boldsymbol{\xi}) M^m(\boldsymbol{\xi}) dS_{\boldsymbol{\xi}} \bar{t}_q^m \\ &+\delta u_b^n \textstyle\int_{S_t} D(\mathbf{x}) N^n(\mathbf{x}) dS_{\mathbf{x}} \int_{S_u} H_{bq}^*(\mathbf{x},\boldsymbol{\xi}) D(\xi) N^m(\boldsymbol{\xi}) dS_{\boldsymbol{\xi}} \bar{u}_q^m \\ &= -\delta u_b^n \textstyle\int_{S_t} D(\mathbf{x}) N^n(\mathbf{x}) dS_{\mathbf{x}} \int_{S_u} G_b^{*q}(\mathbf{x},\boldsymbol{\xi}) M^m(\xi) dS_{\boldsymbol{\xi}} t_q^m \\ &+\delta u_b^n \textstyle\int_{S_t} N^n(\mathbf{x}) dS_{\mathbf{x}} \int_{S_u} n_a(\mathbf{x}) \phi_{ab}^{*q}(\mathbf{x},\boldsymbol{\xi}) M^m(\boldsymbol{\xi}) dS_{\boldsymbol{\xi}} t_q^m \\ &-\delta u_b^n \textstyle\int_{S_t} D(\mathbf{x}) N^n(\mathbf{x}) dS_{\mathbf{x}} \int_{S_t} H_{bq}^*(\mathbf{x},\boldsymbol{\xi}) D(\xi) N^m(\boldsymbol{\xi}) dS_{\boldsymbol{\xi}} u_q^m \end{aligned} \tag{48}$$

Equation (47) and (48) can be written in matrix form:

$$\begin{Bmatrix} \delta \mathbf{t_u} \\ \delta \mathbf{u_t} \end{Bmatrix}^T \begin{bmatrix} \mathbf{A_{uu}} & \mathbf{A_{ut}} \\ \mathbf{A_{tu}} & \mathbf{A_{tt}} \end{bmatrix} \begin{Bmatrix} \mathbf{t_u} \\ \mathbf{u_t} \end{Bmatrix} = \begin{Bmatrix} \delta \mathbf{t_u} \\ \delta \mathbf{u_t} \end{Bmatrix}^T \begin{Bmatrix} \mathbf{b_u} \\ \mathbf{b_t} \end{Bmatrix} \tag{49}$$

or:

$$\mathbf{Ax} = \mathbf{b} \tag{50}$$

$\mathbf{t_u}, \mathbf{u_t}$ are undetermined tractions at S_u, and undetermined displacements at S_t respectively. With simple mathematical manipulations, one can show that the coefficient matrix in (49)is symmetric. However, (49) is not always rank-sufficient. Some constraints may need to be added to the degrees of freedoms in order to uniquely solve the unknown tractions and displacements. This will be discussed in next section in detail. Once the unknowns are solved using (49), the displacements, strains and stresses can be determined using the BIEs as shown in (9) and (17), or those regularized versions as shown in [Han and Atluri (2003)] when $\mathbf{x}$ is approaching to point $\hat{\mathbf{x}}$ on the boundary:

$$\begin{aligned} &u_p(\mathbf{x}) = \int_{\partial\Omega} t_j(\boldsymbol{\xi}) u_j^{*p}(\mathbf{x},\boldsymbol{\xi}) dS_{\boldsymbol{\xi}} - \int_{\partial\Omega} [u_j(\boldsymbol{\xi}) - u_j(\hat{\mathbf{x}})] t_j^{*p}(\mathbf{x},\boldsymbol{\xi}) dS_{\boldsymbol{\xi}} \\ &+ \int_{\Omega} \bar{f}_j(\boldsymbol{\xi}) u_j^{*p}(\mathbf{x},\boldsymbol{\xi}) d\Omega_{\boldsymbol{\xi}} + u_p(\hat{\mathbf{x}}) \end{aligned} \tag{51}$$

$$\begin{aligned} &u_{p,k}(\mathbf{x}) = -\int_{\partial\Omega} [t_j(\xi) - n_i(\boldsymbol{\xi})\sigma_{ij}(\hat{\mathbf{x}})] u_{j,k}^{*p}(\mathbf{x},\boldsymbol{\xi}) dS_{\boldsymbol{\xi}} \\ &- \int_{\partial\Omega} [D(\boldsymbol{\xi}) u_m(\boldsymbol{\xi}) - n_r(\boldsymbol{\xi}) e_{rs} u_{m,s}(\hat{\mathbf{x}})] e_{nk} \sigma_{nm}^{*p}(\mathbf{x},\boldsymbol{\xi}) dS_{\boldsymbol{\xi}} \\ &- \int_{\Omega} \bar{f}_j(\boldsymbol{\xi}) u_{j,k}^{*p}(\mathbf{x},\boldsymbol{\xi}) d\Omega_{\boldsymbol{\xi}} \end{aligned} \tag{52}$$

$$\begin{aligned} &\sigma_{ab}(\mathbf{x}) = -\int_{\partial\Omega} [t_p(\boldsymbol{\xi}) - n_q(\boldsymbol{\xi})\sigma_{pq}(\hat{\mathbf{x}})] \sigma_{ab}^{*p}(\mathbf{x},\boldsymbol{\xi}) dS_{\boldsymbol{\xi}} \\ &- \int_{\partial\Omega} [D(\boldsymbol{\xi}) u_q(\boldsymbol{\xi}) - n_r(\boldsymbol{\xi}) e_{rs} u_{q,s}(\hat{\mathbf{x}})] \Sigma_{abq}^{*}(\mathbf{x},\boldsymbol{\xi}) dS_{\boldsymbol{\xi}} \\ &- \int_{\Omega} \bar{f}_p(\boldsymbol{\xi}) \sigma_{ab}^{*p}(\mathbf{x},\boldsymbol{\xi}) d\Omega_{\boldsymbol{\xi}} + \sigma_{ab}(\hat{\mathbf{x}}) \end{aligned} \tag{53}$$

5 Constraints Applied to Cavities, Edge Cracks, Branching Cracks, and Intersecting Cracks

The discretized symmetric Galerkin BIEs as shown in last section are valid for domains with arbitrary cavities and arbitrary cracks. But this does not mean they are sufficient to solve for the unknowns. For example, when traction boundary conditions are applied to the whole domain, i.e. $S_t = \partial\Omega$,the unknown displacements cannot be defined because of the arbitrary rigid body modes. In this case, one can either fix three proper displacement DOFs to constrain the rigid-body modes, or simply append the constraints that the three rigid-body modes are zero. For a set of points with coordinates (x_k, y_k), displacements for each point $u_i^{(k)}$ can be divided into rigid-body and non-rigid-body parts $\bar{u}_i^{(k)}, \hat{u}_i^{(k)}$:

$$\begin{aligned} \mathbf{u}^{(k)} &= \begin{Bmatrix} u_1^{(k)} \\ u_2^{(k)} \end{Bmatrix} = \begin{Bmatrix} \bar{u}_1^{(k)} \\ \bar{u}_2^{(k)} \end{Bmatrix} + \begin{Bmatrix} \hat{u}_1^{(k)} \\ \hat{u}_2^{(k)} \end{Bmatrix} \\ &= \begin{bmatrix} 1 & 0 & -y_k \\ 0 & 1 & x_k \end{bmatrix} \begin{Bmatrix} \alpha_1 \\ \alpha_2 \\ \alpha_3 \end{Bmatrix} + \begin{Bmatrix} \hat{u}_1^{(k)} \\ \hat{u}_2^{(k)} \end{Bmatrix} \\ &= \mathbf{R}^{(k)} \boldsymbol{\alpha} + \hat{\mathbf{u}}^{(k)} \end{aligned} \tag{54}$$

If we put the displacements of all points in one vector $\mathbf{u}$, we correspondingly obtain the following equation:

$$\mathbf{u} = \mathbf{R}\boldsymbol{\alpha} + \hat{\mathbf{u}} \tag{55}$$

Because of the orthogonality of the rigid-body and the non-rigid-body modes,$\boldsymbol{\alpha}$ can be determined by:

$$\boldsymbol{\alpha} = \left(\mathbf{R}^T\mathbf{R}\right)^{-1}\mathbf{R}^T\mathbf{u} \tag{56}$$

Therefore, when tractions boundary conditions are applied to the whole boundary, one can apply the equation $\left(\mathbf{R}^T\mathbf{R}\right)^{-1}\mathbf{R}^T\mathbf{u} = 0$ to constrain the three rigid-body-modes

A slightly more complex case is when, in addition to $S_t = \partial\Omega$, there are cavities present in the domain. From the symmetric Galerkin BIE (27), one can see that rigid-body-modes of the cavity contribute nothing to the tractions on the boundary. This is different from FEM. However, similar to what we have just discussed here, one can easily append the constraints that the rigid-body-modes of each cavity are equal to the rigid-body modes of the outer boundary. Suppose the displacements of the outer boundary are $\mathbf{u}_0$, and displacements of cavity l are $\mathbf{u_l}$, one can obtain the following constraints:

$$\left(\mathbf{R}_0^T\mathbf{R}_0\right)^{-1}\mathbf{R}_0^T\mathbf{u}_0 - \left(\mathbf{R}_l^T\mathbf{R}_l\right)^{-1}\mathbf{R}_l^T\mathbf{u}_l = 0 \tag{57}$$

$\mathbf{R}_0, \mathbf{R}_l$ depend on the coordinates of the points in the outer boundary and those of the cavity, as shown in (54).

One may also encounter the case that some cracks intersect with the outer boundary or some cavities (edge cracks). In this case, some constraints of displacement compatibility should be applied. In order not to bring any ambiguity, we firstly define a positive direction of each crack L_i. The corresponding L_i^+, L_i^- are defined as follows: if one is walking along in the positive direction of the crack L_i, L_i^+ is on his left-hand side, and L_i^- is on his right-hand side. When modeling the problem with SGBEM, at the intersecting node k, discontinuous displacement vectors are assumed on the global boundary of the crack, $u_i^{(k)+}, u_i^{(k)-}$; thus, $\Delta u_i^{(k)}$ is assumed on the crack surface. The compatibility condition which needs to be applied is:

$$\Delta u_i^{(k)} - u_i^{(k)+} + u_i^{(k)-} = 0 \tag{58}$$

Another more interesting problem is that when some cracks are branching or intersecting. As shown in Fig. 4, when some cracks have a common node k, we

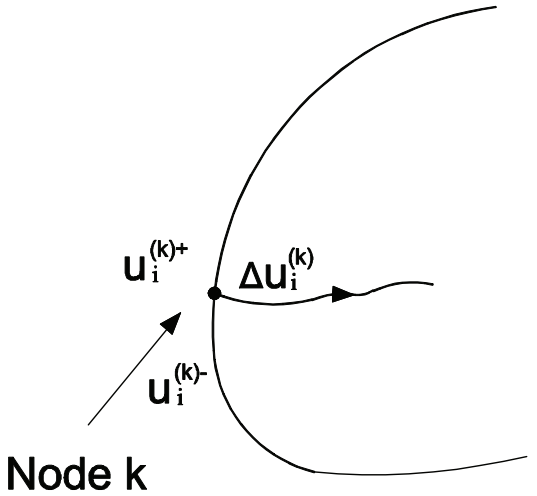

Figure 3: Treatment of edge cracks

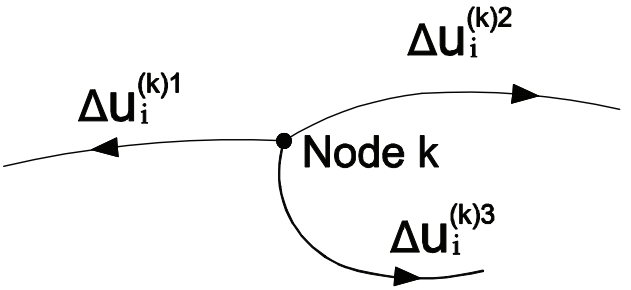

Figure 4: Treatment of branching/intersecting cracks

assume $\Delta u_i^{(k)n}, n = 1,2,3...$ for each branching/intersecting crack. From the theory of Somigliana dislocations, one can easily find the compatibility condition:

$$\sum_n s_n \Delta u_i^{(k)n} = 0 \tag{59}$$

s_n is defined as follows: when one walks along crack n, from the intersecting node to further locations, if one is walking in the positive direction of the crack, then $s_n = 1$, otherwise $s_n = -1$.

From the discussion of this section, we can see that all the constraints are in the form of:

$$\mathbf{Gx} = \mathbf{0} \tag{60}$$

where $\mathbf{x}$ is a vector containing all the unkown displacements and tractions.

One can apply these constraints by using the traditional method of Lagrange multipliers, leading to a system of well-defined equations:

$$\begin{bmatrix} \mathbf{A} & \mathbf{G^T} \\ \mathbf{G} & \mathbf{0} \end{bmatrix} \begin{Bmatrix} \mathbf{x} \\ \mathbf{y} \end{Bmatrix} = \begin{Bmatrix} \mathbf{b} \\ \mathbf{0} \end{Bmatrix} \tag{61}$$

6 Evaluating the Stress Intensity Factors for Cracks, and Modeling Their Fatigue Growth

For 2D SGBEM, the boundary $\partial\Omega$ is discretized by boundary elements. Usual two-node linear elements and three-node quadratic elements can be used at locations other than crack tips. Two-node square-root-singular elements as in [Park and Atluri(1998)], and three-node quarter-point singular element as in many studies, e.g. [Frangi and Novati (1996)], can be used at crack tips to improve accuracy. In this study, two-node linear elements and two-node crack-tip elements are used for demonstration purposes.

Stress intensity factors can be directly evaluated using crack-tip opening displacements:

$$\begin{aligned} K_1 &= \tfrac{E}{8(1-\bar{\nu}^2)} \lim_{r\to 0} \Delta u_2 \sqrt{\tfrac{2\pi}{r}} \\ K_2 &= \tfrac{E}{8(1-\bar{\nu}^2)} \lim_{r\to 0} \Delta u_1 \sqrt{\tfrac{2\pi}{r}} \end{aligned} \tag{62}$$

where Δu_k is the crack tip opening displacements in the local Cartesian coordinate system aligned to the crack surface. However, the stress intensity factor of this method strictly depends on the solution of crack tip displacements, which might need a fine mesh to obtain an accurate solution.

In this study, we use path-independent integrals to evaluate the stress intensity factors and the fatigue growth of cracks. When crack-surface is traction free and body-force is negligible, the vector J-integral is:

$$J_l = \int_{\Gamma} n_i M_{il} dS \tag{63}$$

where M_{il} is Eshelby's energy momentum tensor, see [Eshelby (1951,1975)]:

$$M_{il} = W\delta_{il} - \sigma_{ij} u_{j,l} \tag{64}$$

In the crack-tip local Cartesian coordinate system, we calculate the stress intensityfactors as:

$$\begin{aligned} K_1 &= \frac{\delta_1}{\delta}\sqrt{\frac{J_1 E}{(1-\bar{\nu}^2)}} \\ K_2 &= \frac{\delta_2}{\delta}\sqrt{\frac{J_1 E}{(1-\bar{\nu}^2)}} \\ \delta_1 &= \lim_{r\to 0} \Delta u_2 \sqrt{\frac{1}{r}} \\ \delta_2 &= \lim_{r\to 0} \Delta u_1 \sqrt{\frac{1}{r}} \\ \delta &= \sqrt{\delta_1^2 + \delta_2^2} \end{aligned} \tag{65}$$

For the fatigue growth of the cracks, we consider crack growth rate to be a function of the effective stress intensity factor:

$$\frac{da}{dN} = f(\Delta K) \tag{66}$$

Two models are used in this study: the Paris law

$$\frac{da}{dN} = C(\Delta K)^n \tag{67}$$

and the Forman law

$$\frac{da}{dN} = \frac{C(\Delta K)^n}{(1-R)K_c - \Delta K} \tag{68}$$

where K_c is the critical stress intensity factor.

The effective stress intensity factor is determined by the energy relation:

$$\begin{aligned} \Delta K &= \sqrt{\frac{\Delta J E}{(1-\bar{\nu}^2)}} \\ \Delta J &= \sqrt{\Delta J_1^2 + \Delta J_2^2} \end{aligned} \tag{69}$$

Instead of using maximum stress criteria or minimum strain energy criteria, we follow the continuum theory of defects, which involve the concept of the energy momentum tensor of Eshelby. The propagation angle is simply assumed to be the direction of the vector J-integral:

$$\alpha = \tan^{-1} \frac{J_2}{J_1}.$$

Some numerical examples will be shown in next section.

7 Numerical Examples for Global SGBEM

7.1 Embedded Cracks

Firstly, we solve the problem of an embedded through-the-thickness crack. A crack of length 20 cm is located at the center of a plate of 1m width and 2m height. Normal stress, 50MPa is applied on the upper edge. This is shown in Fig. 5 with a = 0.1, b = 0.5, d = 0.5, h =1, and σ = 50. This problem will be solved for 2 cases. For the first case, we use only one element for each side of the plate and 2 elements to mesh the crack.For the second case, we use two elements to mesh each side of the plate and 4 elements to mesh the crack.We compare the computed stress intensity factor to those in analytical solutions in [Anderson (2005)].

$$K_1 = \sigma\sqrt{\pi a}\sqrt{\frac{2b}{\pi a}\tan\frac{\pi a}{2b}} \tag{70}$$

Table 1: Computational results for the center crack in Fig. 5

	Mesh	SGBEM	Analytical	Error
K1	1	28.16	28.50	1.19%
	2	28.44	28.50	0.21%

We can see that, for this simple problem, we can obtain an accuracy of 1.19% error, even with a coarse mesh of only 7 nodes (the most coarse mesh possible). And when 13 nodes is used, the error decreases drastically to 0.21%.

The second problem we solve is a plate with two off-aligned cracks, as shown in Fig. 6. The plate is 40mm$\times$80mm. The two parallel cracks are with dimensions of a=1.27mm, e/f=0.3 and 2a/d=0.8. The crack without tip A is located on the center of the plate. An evenly distributed tensile loading of 400Pa is applied to the upper and lower edges. 2 elements are used for each edge of the plate, and 10 elements

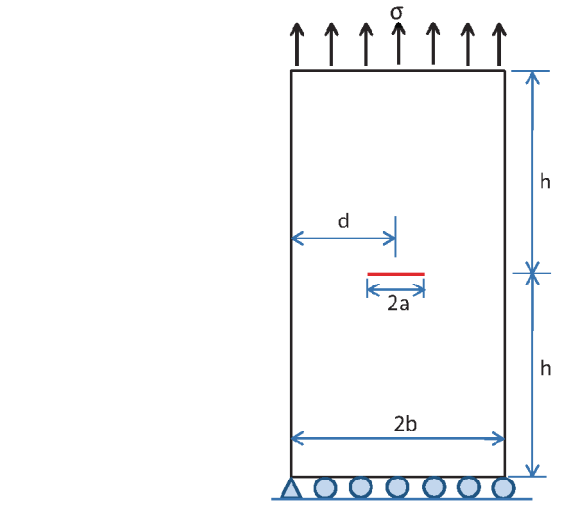

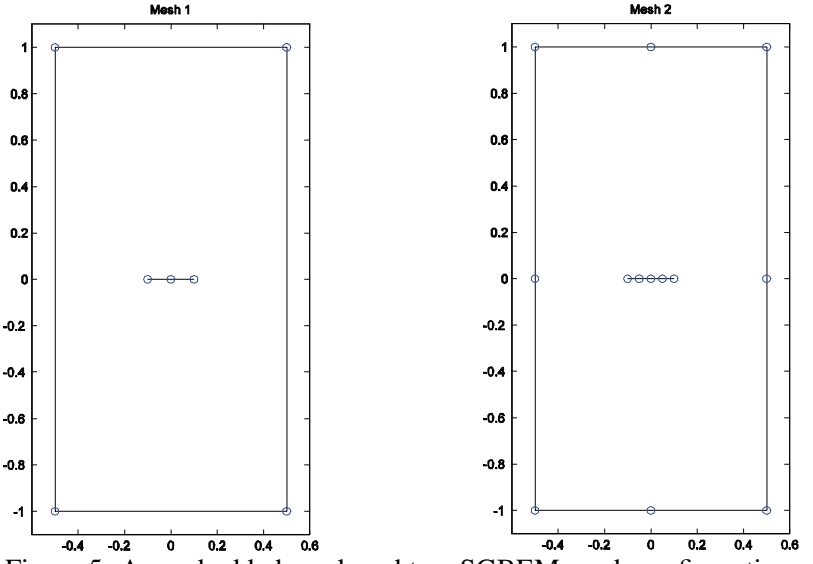

Figure 5: An embedded crack and two SGBEM mesh configuration

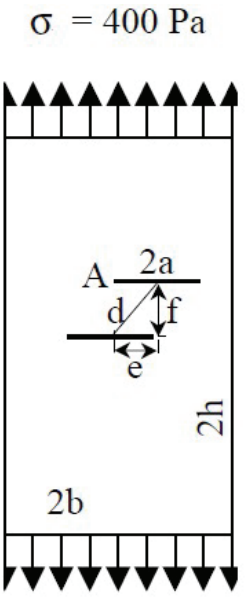

Figure 6: Two off-aligned cracks

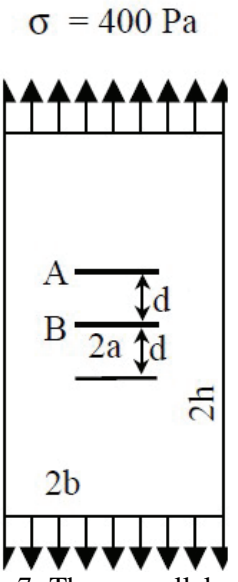

Figure 7: Three parallel cracks

Table 2: Computational results for the two off-aligned cracks in Fig. 6

	SGBEM	Handbook	Error
K1A	671.220	671.144	0.18%

are used for each crack. Totally 30 nodes are used. K1 for crack tip A are compared to the Handbook solution [Murakami (1987)] in Tab. 2.

Another example is selected: three parallel cracks aligned normally to the tensile direction. A schematic of the problem is shown below in Fig. 7. The plate is 40mm×80mm. The three parallel cracks are with dimensions of a=1.27mm, d=3.175mm the crack B is located at the center of the plate. An evenly distributed tensile loading of 400Pa is applied to the upper and lower edges. 2 elements are used for each edge of the plate, and 10 elements are used for each crack. Totally 41 nodes are used. K1 for crack tip A are compared to the Handbook solution [Murakami (1987)] in Tab. 3.

Table 3: Computationalresults for the three parallel cracks in Fig. 7

	SGBEM	Handbook	Error
K1A	679.029	679.550	0.08%
K1B	600.659	599.235	0.23%

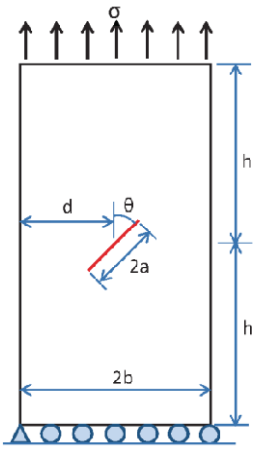

Figure 8: An Embedded Slanted Crack

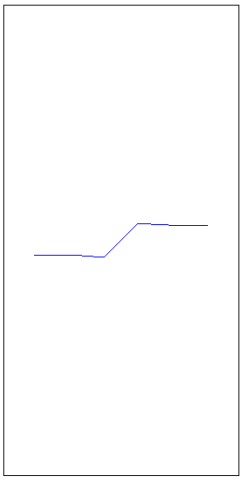

Figure 9: Final shape of the embedded slant crack shown in Fig. 8, after fatigue-crack-growth

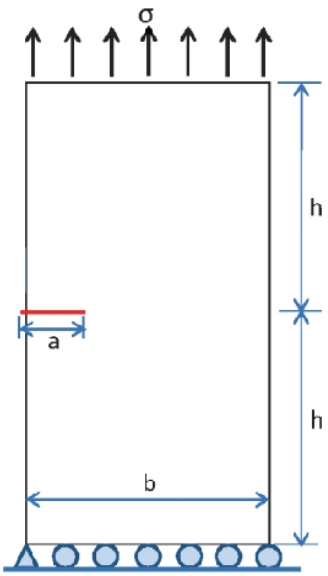

Figure 10: An Edge Crack

Now we solve the problem of an embedded through-the-thickness slanted crack. A crack of length 20 cm is located at the center of a plate of 1m width and 2m height. The slant angle is $\pi/4$. Normal stress 50MPa is applied on the upper edge. This is shown in Fig. 8 with a = 0.1, b = 0.5, d = 0.5, h =1, and σ = 50.Material properties are $E = 205Gpa, v = 0.3$. Ten elements are used for each edge of the plate, and 10 elements are used for each crack. Totally 43 nodes are used for the original mesh. The number of analysis steps used in fatigue-crack-growth analysis is 30. The total simulated crack growth is equal to 0.3. Thus, in each step the crack increment is 0.3/30 = 0.01. The Paris fatigue crack-growth equation is used. The parameters of the equation are: C = $6.9 \times 10^{-12}$and n = 3. Computational results show that after 629398 cycles, the slant crack has grown to a mode 1 dominant crack as shown in Fig. 9.

7.2 Edge Cracks

An edge crack of length a = 0.2 in a finite plate as shown in Fig.10 having dimensions: b = h = 1 and loaded by a uniform axial stress σ = 50, is considered.We use 8 elements to mesh each edge of the plate. The edge crack is meshed using 10 elements. Totally 43 nodes are used. The computational results are compared to the handbook solution in Tab. 4.

Table 4: Computational Results for the edge crack in Fig. 10

	SGBEM	Handbook	Error
K1	54.210	54.418	0.38%

Another example is selected: edge cracks emanating from a circular fastener hole. A schematic of the problem is shown in Figure 11. The plate is 50.8mm$\times$101.6mm. A circular hole with R=6.35mm is located at the center of the plate, and cracks emanate from the hole with a=6.604mm. An evenly distributed tensile loading of 82.74Pa is applied to the upper and lower edge. 4 elements are used to mesh each edge of the plate. 48 elements are used to mesh the circle. 10 elements are used to mesh each crack. Totally 86 nodes are used. The computational results are compared to the handbook solution in Tab. 6.

Table 5: Computational Results for the cracks in Fig. 11

	SGBEM	Handbook	Error
K1	249.55	248.47	0.43%

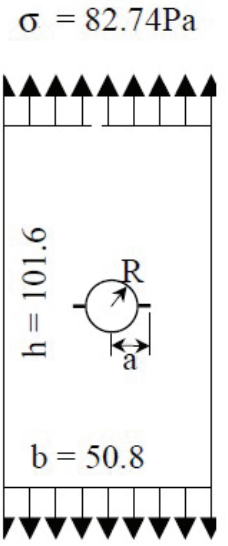

Figure 11: Cracks Emanating from a Circular Fastener Hole

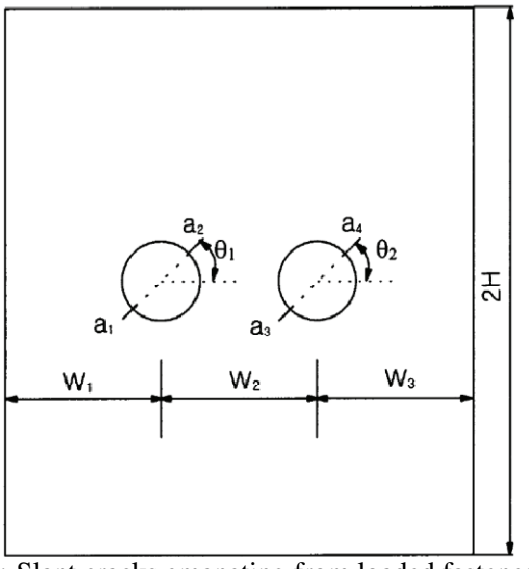

Figure 12: Slant cracks emanating from loaded fastener holes

We also model the mixed mode fatigue growth of multiple slanted cracks emanating from fastener-holes in an aircraft fuselage lap-joint. Fig. 12 shows the geometry of the plate with the two holes and the cracks emanating from them. The geometric parameters are as follows:

H = 4 inch, $W_1 = W_3$ = 1.5 inch, W_2 = 1 inch.

The radius of the holes: R = 0.0805 inch.

The initial crack lengths: $a_1 = a_2 = a_3 = a_4$= 0.03 inch.

Cracks' angles: $\theta_1 = \theta_2 = 30^o$.

The material is 2024-T3 aluminum alloy whose properties are:

E = 10.6×10^6, and v = 0.33.

The fatigue behavior is expressed by Forman's equation. Here, Kc= 83,000 psi, C = 3×10^{-13} and n = 3. Uniform tension is applied on the upper andlower edges.The maximum stress is 12 ksi and the stress ratio R = 0.1. The initial mesh configuration has 10 elements for each edge of the plate, 32 elements for each hole, and 5 elements for each crack. Totally 128 nodes are used. We are applying 50 analysis steps, with varying number of cycles in each step so that the crack growth increment in any step is equal to 0.014, giving, after the 50 steps, a growth of 0.7. Computational results show that totally 71218 cycles are needed. And the final results are shown in Fig. 13.

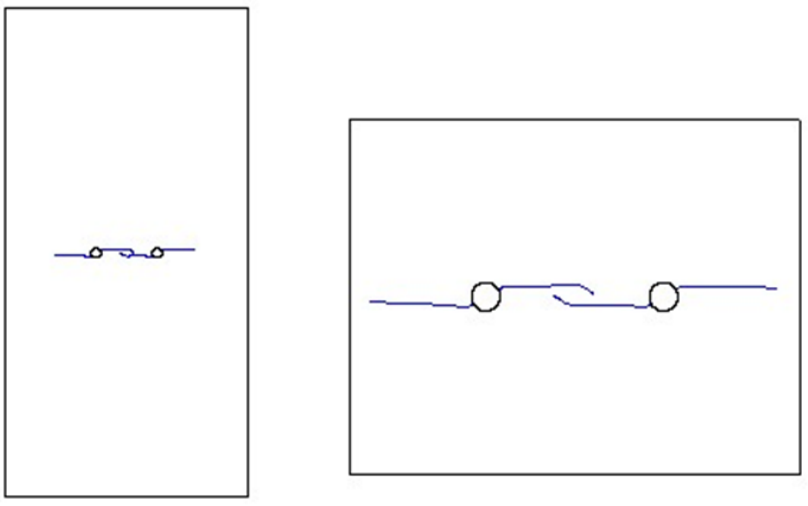

Figure 13: The final shapes of cracksfrom fastener holes of Fig. 12, after fatigue growth

7.3 Branching and Intersecting Cracks

We also show that the SGBEM presented in this study can model branching and intersecting cracks accurately and efficiently.

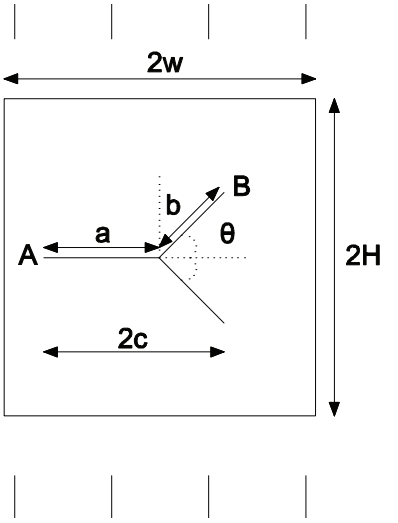

Figure 14: A branching crack

We firstly study the case of a branching crack, as shown in Fig. 14. The geometrical parameters are: a=b=0.1, θ = 45°, and H=w=4. Uniform stress $\sigma = 50$ is applied to the upper and lower edges. Material properties are $E = 205Gpa, v = 0.3$. 4 elements are used for each side of the plate, and 10 elements are used for each crack segment. Totally 45 nodes are used for the initial configuration. F_{1A}, F_{1B}, F_{2B} are defined as:

$$\begin{aligned} F_{1A} &= \frac{K_{1A}}{\sigma\sqrt{\pi a}} \\ F_{1B} &= \frac{K_{1B}}{\sigma\sqrt{\pi b}} \\ F_{2B} &= \frac{K_{2B}}{\sigma\sqrt{\pi b}} \end{aligned} \tag{71}$$

Computational results are shown in Tab. 7, and are compared to those of [Chen and Hasebe (1995)].

We also study the fatigue growth the branching crack. The number of analysis steps is 30. The total crack growth = 0.3 for each crack tip A. Thus, in each step the crack increment is 0.3/30 = 0.01. The Paris equation is used. The parameters of the equation are: C = $6.9 \times 10^{-12}$and n = 3. Computational results show that after

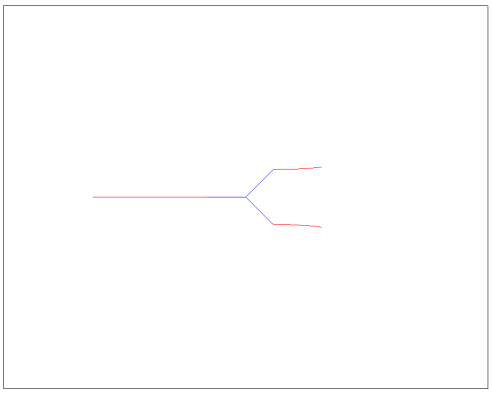

Figure 15: The final shape of the branching crack of Fig. 14, after fatigue growth

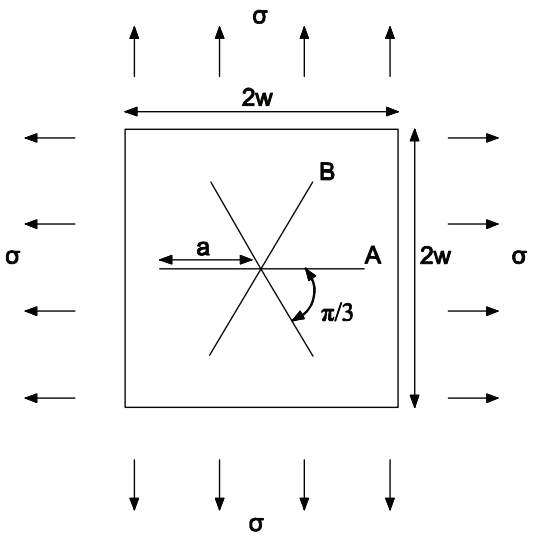

Figure 16: A star crack

Table 6: Computational Results for the branching crack in Fig. 14

	SGBEM	Chen and Hasebe (1995)	Error
F1A	0.964	0.964	0.00%
F1B	0.456	0.457	0.22%
F2B	0.469	0.467	0.43%

798159 cycles, the branching crack has grown to a final shape as shown in Fig. 15, as opposed to the single slant crack as shown in Fig. 8-9.

In the last example, we consider a star-shaped crack as shown in Fig. 16.

Table 7: Computational Results for the star crackshown in Fig. 16

	SGBEM	Chen and Hasebe (1995)	Error
F1A	0.659	0.659	0.00%
F1B	0.659	0.659	0.00%

The geometrical parameters are: a=0.1, $\theta = 45^{\circ}$, and H=w=4. Uniform stress $\sigma =$ 50 is applied to each edge. 4 elements are used for each side of the plate, and 10 elements are used for each crack segment. Totally 104 nodes are used. F_{1A}, F_{1B} are defined as:

$$\begin{aligned} F_{1A} &= \frac{K_{1A}}{\sigma\sqrt{\pi a}} \\ F_{1B} &= \frac{K_{1B}}{\sigma\sqrt{\pi a}} \end{aligned} \tag{72}$$

Computational results are shown in Tab. 8, and are in good agreement to those of [Chen and Hasebe (1995)].

7.4 Super Elements Developed by using the Symmetric Galerkin BIEs

Global SGBEM has shown its accuracy and efficiency in solving defective solids with arbitrary embedded, edge, branching and intersecting cracks. However, because SGBEM always give a system of equations with fully populated coefficient matrices, it is not suitable for modeling large-scale structures, e.g. bridges, automobiles, aircrafts. Therefore, it is beneficial to model a global structure with finite elements, and model a local subdomain with SGBEM. [Han and Atluri (2003)] use the Schwartz-Neumann alternating method without a direct coupling of SGBEM and FEM, and have shown the accuracy and efficiency of their method, in calculating the stress intensity factors of 3D non-planar cracks, and modeling of their non-planar fatigue growth. In this section, we develop a "Super Element" of the

local subdomain, with arbitrary cavities and cracks. The developed super element has a stiffness matrix and a force vector which corresponds to those of the traditional FEM. The stiffness matrix is positive semi-definite with the correct number of rigid body modes. And the developed equations of the "super element" can be directly coupled with the usual finite element equations using the usual assembly procedure.

Because the Super Elements with and without cracks are slightly different in their formulation, they are presented in the following two subsections respectively.

7.5 Super Element without Cracks

In this section, we only consider a subdomain without cracks.

In the global SGBEM as shown in section 4, unknown displacements are expressed in terms of boundary element shape functions at S_t, and unknown tractions are assumed at S_u. For the global SGBEM, the displacement BIE is used at S_u, and the traction BIE is used at S_t. However, for the local subdomain Ω, we firstly do not distinguish what types of boundary conditions are considered, and assume displacements as $u_i = \mathbf{N}\mathbf{q}_i$ andtractions as $t_i = \mathbf{M}\mathbf{p}_i$ at the whole boundary $\partial\Omega$ of the local subdomain. By using both displacement BIE (33) and traction BIE (29) for the whole $\partial\Omega$, we have:

$$\begin{aligned}
&-\tfrac{1}{2}\delta\mathbf{p}_j^T \int_{\partial\Omega} \mathbf{M}^T(\mathbf{x})\mathbf{N}(\mathbf{x})dS_x\mathbf{q}_j \\
&= -\delta\mathbf{p}_p^T \int_{\partial\Omega} \mathbf{M}^T(\mathbf{x})dS_x \int_{\partial\Omega} u_j^{*p}(\mathbf{x},\boldsymbol{\xi})\mathbf{M}(\boldsymbol{\xi})dS_{\boldsymbol{\xi}}\mathbf{p}_j \\
&-\delta\mathbf{p}_p^T \int_{\partial\Omega} \mathbf{M}^T(\mathbf{x})dS_x \int_{\partial\Omega} G_j^{*p}(\mathbf{x},\boldsymbol{\xi})D(\boldsymbol{\xi})\mathbf{N}(\xi)dS_{\boldsymbol{\xi}}\mathbf{q}_j \\
&-\delta\mathbf{p}_p^T \int_{\partial\Omega} \mathbf{M}^T(\mathbf{x})dS_x \int_{\partial\Omega} n_i(\xi)\phi_{ij}^{*p}(\mathbf{x},\boldsymbol{\xi})\mathbf{N}(\xi)dS_{\boldsymbol{\xi}}\mathbf{q}_j
\end{aligned} \tag{73}$$

$$\begin{aligned}
&\tfrac{1}{2}\delta\mathbf{q}_b^T \int_{\partial\Omega} \mathbf{N}(\mathbf{x})^T\mathbf{M}(\mathbf{x})dS_{\mathbf{x}}\mathbf{p}_b \\
&= -\delta\mathbf{q}_b^T \int_{\partial\Omega} D(\mathbf{x})\mathbf{N}^T(\mathbf{x})dS_{\mathbf{x}} \int_{\partial\Omega} G_b^{*q}(\mathbf{x},\boldsymbol{\xi})\mathbf{M}(\xi)dS_{\boldsymbol{\xi}}\mathbf{p}_q \\
&+\delta\mathbf{q}_b^T \int_{\partial\Omega} \mathbf{N}(\mathbf{x})^T dS_{\mathbf{x}} \int_{\partial\Omega} n_a(\mathbf{x})\phi_{ab}^{*q}(\mathbf{x},\boldsymbol{\xi})\mathbf{M}(\boldsymbol{\xi})dS_{\boldsymbol{\xi}}\mathbf{p}_q \\
&-\delta\mathbf{q}_b^T \int_{\partial\Omega} D(\mathbf{x})\mathbf{N}^T(\mathbf{x})dS_{\mathbf{x}} \int_{\partial\Omega} H_{bq}^*(\mathbf{x},\boldsymbol{\xi})D(\xi)\mathbf{N}(\boldsymbol{\xi})dS_{\boldsymbol{\xi}}\mathbf{q}_q
\end{aligned} \tag{74}$$

Without ambiguity, one can rewrite (73) and (74), as:

$$-\frac{1}{2}\delta\mathbf{p}^T\mathbf{U}\mathbf{q} = \delta\mathbf{p}^T\mathbf{P}\mathbf{P}\mathbf{p} + \delta\mathbf{p}^T\mathbf{P}\mathbf{Q}\mathbf{q} \tag{75}$$

$$\frac{1}{2}\delta\mathbf{q}^T\mathbf{T}\mathbf{p} = \delta\mathbf{q}^T\mathbf{Q}\mathbf{P}\mathbf{p} + \delta\mathbf{q}^T\mathbf{Q}\mathbf{Q}\mathbf{q} \tag{76}$$

where(75) corresponds to (73), and (76) corresponds to (74).

From the property of SGBEM, or by some trivial math manipulation, one can see that, if $\mathbf{M} = \mathbf{N}$, then:

$$\begin{aligned} &\mathbf{U} = \mathbf{T}^T \\ &\mathbf{PP} = \mathbf{PP}^T \\ &\mathbf{QQ} = \mathbf{QQ}^T \\ &\mathbf{PQ} = \mathbf{QP}^T \end{aligned} \tag{77}$$

Using a slight manipulation, one can rewrite (75)and (76), as:

$$\mathbf{0} = \delta\mathbf{p}^T \mathbf{PPp} + \delta\mathbf{p}^T \left(\mathbf{PQ} + \frac{1}{2}\mathbf{U} \right) \mathbf{q} \tag{78}$$

$$\delta\mathbf{q}^T \mathbf{Tp} = \delta\mathbf{q}^T \left(\mathbf{QP} + \frac{1}{2}\mathbf{T} \right) \mathbf{p} + \delta\mathbf{q}^T \mathbf{QQq} \tag{79}$$

Because $\delta\mathbf{p}$ is arbitrary (unlike $\delta\mathbf{q}$), we can use static condensation of (78)(79) to obtain:

$$\delta\mathbf{q}^T \mathbf{Tp} = \delta\mathbf{q}^T \left[\mathbf{QQ} - \left(\mathbf{QP} + \frac{1}{2}\mathbf{T} \right) \mathbf{PP}^{-1} \left(\mathbf{PQ} + \frac{1}{2}\mathbf{U} \right) \right] \mathbf{q} \tag{80}$$

From the properties in (77), we can see that the matrix in the right-hand side is symmetric.

One more interesting observation is that:

$$\begin{aligned} &\delta\mathbf{q}^T \mathbf{Tp} = \delta\mathbf{q}_b^T \int_{\partial\Omega} \mathbf{N}(\mathbf{x})^T \mathbf{M}(\mathbf{x}) dS_{\mathbf{x}} \mathbf{p}_b \\ &= \delta\mathbf{q}_b^T \int_{\partial\Omega} \mathbf{N}(\mathbf{x})^{\mathbf{T}} \mathbf{t}_{\mathbf{b}}(\mathbf{x}) dS_{\mathbf{x}} \\ &= \delta\mathbf{q}^T \mathbf{Q} \end{aligned} \tag{81}$$

where the vector $\mathbf{Q}$ has the exact form of the generalized "force vector" in FEM. Therefore, it is clear that the right hand side of (80) has the physical meaning of the variation of strain-energy of Ω, and the symmetric matrix can be considered as the "stiffness matrix" of the local subdomain. (80) can be therefore written as:

$$\delta\mathbf{q}^T \mathbf{Q} = \delta\mathbf{q}^T \mathbf{Kq} \tag{82}$$

For numerical implementation, one can simply evaluate the stiffness matrix of the local subdomain as:

$$\mathbf{K} = \mathbf{QQ} - \left(\mathbf{QP} + \frac{1}{2}\mathbf{T} \right) \mathbf{PP}^{-1} \left(\mathbf{PQ} + \frac{1}{2}\mathbf{U} \right) \tag{83}$$

One can also evaluate the force vector $\mathbf{Q}$ using the usual FEM procedure. Hence, the local subdomain can be treated as a "super element", and can be directly coupled with the FEM of the global structure using the usual assembly procedure.

7.6 SGBEM Super Element with Cracks

The SGBEM Super Element is developed in the previous section for a subdomain without cracks. However, when cracks are present, some modifications are necessary. This is because of the fact that, the weakly-singular BIEs developed in section 2, can only allow users to consider cracks as part of the traction boundary, where unkowns are the displacement discontinuity Δu_i at S_c. Crack surface tractions are considered to be known (equal to 0 for example). When Δu_i are considered as unkowns, traction BIE, in a symmetric Galerkin weak form, is applied to the crack surface. On the other hand, if one consider crack surface tractions as unkowns, displacement BIE as developed in section 2 are not useful at the crack surface.

Therefore, the following modifications are made. Consider the boundary of domain Ω which can be divided into S_b and S_c, where S_b is the summation of all the closed contours representing the outer boundary and the inner cavities. We assume both unknown displacements $u_i = \mathbf{N}\mathbf{q}_i$ and tractions $t_i = \mathbf{M}\mathbf{p}_i$ at the whole boundary S_b, and we only assume displacement jumps at the crack surface S_c as $\Delta u_i = \mathbf{L}\mathbf{r}_i$. Then we write down the following equations:

$$
\begin{aligned}
&-\tfrac{1}{2}\delta\mathbf{p}_j^T \textstyle\int_{S_b} \mathbf{M}^T(\mathbf{x})\mathbf{N}(\mathbf{x})dS_x\mathbf{q}_j \\
&= -\delta\mathbf{p}_p^T \textstyle\int_{S_b} \mathbf{M}^T(\mathbf{x})dS_x \int_{S_b} u_j^{*p}(\mathbf{x},\boldsymbol{\xi})\mathbf{M}(\boldsymbol{\xi})dS_{\boldsymbol{\xi}}\mathbf{p}_j \\
&-\delta\mathbf{p}_p^T \textstyle\int_{S_b} \mathbf{M}^T(\mathbf{x})dS_x \int_{S_b} G_j^{*p}(\mathbf{x},\boldsymbol{\xi})D(\xi)\mathbf{N}(\boldsymbol{\xi})dS_{\boldsymbol{\xi}}\mathbf{q}_j \\
&-\delta\mathbf{p}_p^T \textstyle\int_{S_b} \mathbf{M}^T(\mathbf{x})dS_x \int_{S_b} n_i(\boldsymbol{\xi})\phi_{ij}^{*p}(\mathbf{x},\boldsymbol{\xi})\mathbf{N}(\boldsymbol{\xi})dS_{\boldsymbol{\xi}}\mathbf{q}_j \\
&-\delta\mathbf{p}_p^T \textstyle\int_{S_b} \mathbf{M}^T(\mathbf{x})dS_x \int_{S_c} G_j^{*p}(\mathbf{x},\boldsymbol{\xi})D(\xi)\mathbf{L}(\boldsymbol{\xi})dS_{\boldsymbol{\xi}}\mathbf{r}_j \\
&-\delta\mathbf{p}_p^T \textstyle\int_{S_b} \mathbf{M}^T(\mathbf{x})dS_x \int_{S_c} n_i(\boldsymbol{\xi})\phi_{ij}^{*p}(\mathbf{x},\boldsymbol{\xi})\mathbf{L}(\boldsymbol{\xi})dS_{\boldsymbol{\xi}}\mathbf{r}_j
\end{aligned}
\tag{84}
$$

$$
\begin{aligned}
&\tfrac{1}{2}\delta\mathbf{q}_b^T \textstyle\int_{S_b} \mathbf{N}(\mathbf{x})^T\mathbf{M}(\mathbf{x})dS_{\mathbf{x}}\mathbf{p}_b \\
&= -\delta\mathbf{q}_b^T \textstyle\int_{S_b} D(\mathbf{x})\mathbf{N}^T(\mathbf{x})dS_{\mathbf{x}} \int_{S_b} G_b^{*q}(\mathbf{x},\boldsymbol{\xi})\mathbf{M}(\boldsymbol{\xi})dS_{\boldsymbol{\xi}}\mathbf{p}_q \\
&+\delta\mathbf{q}_b^T \textstyle\int_{S_b} \mathbf{N}(\mathbf{x})^T dS_{\mathbf{x}} \int_{S_b} n_a(\mathbf{x})\phi_{ab}^{*q}(\mathbf{x},\boldsymbol{\xi})\mathbf{M}(\boldsymbol{\xi})dS_{\boldsymbol{\xi}}\mathbf{p}_q \\
&-\delta\mathbf{q}_b^T \textstyle\int_{S_b} D(\mathbf{x})\mathbf{N}^T(\mathbf{x})dS_{\mathbf{x}} \int_{S_b} H_{bq}^*(\mathbf{x},\boldsymbol{\xi})D(\boldsymbol{\xi})\mathbf{N}(\boldsymbol{\xi})dS_{\boldsymbol{\xi}}\mathbf{q}_q \\
&-\delta\mathbf{q}_b^T \textstyle\int_{S_b} D(\mathbf{x})\mathbf{N}^T(\mathbf{x})dS_{\mathbf{x}} \int_{S_c} H_{bq}^*(\mathbf{x},\boldsymbol{\xi})D(\boldsymbol{\xi})\mathbf{L}(\boldsymbol{\xi})dS_{\boldsymbol{\xi}}\mathbf{r}_q
\end{aligned}
\tag{85}
$$

$$
\begin{aligned}
&\delta\mathbf{r}_b^T \textstyle\int_{S_c} \mathbf{L}(\mathbf{x})^T\bar{t}_b(\mathbf{x})dS_{\mathbf{x}} \\
&= -\delta\mathbf{r}_b^T \textstyle\int_{S_c} D(\mathbf{x})\mathbf{L}^T(\mathbf{x})dS_{\mathbf{x}} \int_{S_b} G_b^{*q}(\mathbf{x},\boldsymbol{\xi})\mathbf{M}(\boldsymbol{\xi})dS_{\boldsymbol{\xi}}\mathbf{p}_q \\
&+\delta\mathbf{r}_b^T \textstyle\int_{S_c} \mathbf{L}(\mathbf{x})^T dS_{\mathbf{x}} \int_{S_b} n_a(\mathbf{x})\phi_{ab}^{*q}(\mathbf{x},\boldsymbol{\xi})\mathbf{M}(\boldsymbol{\xi})dS_{\boldsymbol{\xi}}\mathbf{p}_q \\
&-\delta\mathbf{r}_b^T \textstyle\int_{S_c} D(\mathbf{x})\mathbf{L}^T(\mathbf{x})dS_{\mathbf{x}} \int_{S_b} H_{bq}^*(\mathbf{x},\boldsymbol{\xi})D(\boldsymbol{\xi})\mathbf{N}(\boldsymbol{\xi})dS_{\boldsymbol{\xi}}\mathbf{q}_q \\
&-\delta\mathbf{r}_b^T \textstyle\int_{S_c} D(\mathbf{x})\mathbf{L}^T(\mathbf{x})dS_{\mathbf{x}} \int_{S_c} H_{bq}^*(\mathbf{x},\boldsymbol{\xi})D(\boldsymbol{\xi})\mathbf{L}(\boldsymbol{\xi})dS_{\boldsymbol{\xi}}\mathbf{r}_q
\end{aligned}
\tag{86}
$$

Without ambiguity, one can rewrite these equations as:

$$
-\frac{\mathbf{1}}{\mathbf{2}}\delta\mathbf{p}^{\mathbf{T}}\mathbf{U}\mathbf{q} = \delta\mathbf{p}^{\mathbf{T}}\mathbf{P}\mathbf{P}\mathbf{p} + \delta\mathbf{p}^{\mathbf{T}}\mathbf{P}\mathbf{Q}\mathbf{q} + \delta\mathbf{p}^{\mathbf{T}}\mathbf{P}\mathbf{R}\mathbf{r} \tag{87}
$$

$$\frac{1}{2}\delta\mathbf{q}^T\mathbf{T}\mathbf{p} = \delta\mathbf{q}^T\mathbf{Q}\mathbf{P}\mathbf{p} + \delta\mathbf{q}^T\mathbf{Q}\mathbf{Q}\mathbf{q} + \delta\mathbf{q}^T\mathbf{Q}\mathbf{R}\mathbf{r} \tag{88}$$

$$\delta\mathbf{r}^T\mathbf{R} = \delta\mathbf{r}^T\mathbf{R}\mathbf{P}\mathbf{p} + \delta\mathbf{r}^T\mathbf{R}\mathbf{Q}\mathbf{q} + \delta\mathbf{r}^T\mathbf{R}\mathbf{R}\mathbf{r} \tag{89}$$

One can rewrite these equations as:

$$\mathbf{0} = \delta\mathbf{p}^T\mathbf{P}\mathbf{P}\mathbf{p} + \delta\mathbf{p}^T\left(\mathbf{P}\mathbf{Q} + \frac{1}{2}\mathbf{U}\right)\mathbf{q} + \delta\mathbf{p}^{\mathbf{T}}\mathbf{P}\mathbf{R}\mathbf{r} \tag{90}$$

$$\delta\mathbf{q}^T\mathbf{Q} = \delta\mathbf{q}^T\left(\mathbf{Q}\mathbf{P} + \frac{1}{2}\mathbf{T}\right)\mathbf{p} + \delta\mathbf{q}^T\mathbf{Q}\mathbf{Q}\mathbf{q} + \delta\mathbf{q}^T\mathbf{Q}\mathbf{R}\mathbf{r} \tag{91}$$

$$\delta\mathbf{r}^T\mathbf{R} = \delta\mathbf{r}^T\mathbf{R}\mathbf{P}\mathbf{p} + \delta\mathbf{r}^T\mathbf{R}\mathbf{Q}\mathbf{q} + \delta\mathbf{r}^T\mathbf{R}\mathbf{R}\mathbf{r}$$

Following the same static condensation procedure, we obtain the following equations:

$$\begin{pmatrix}\delta\mathbf{q}\\ \delta\mathbf{r}\end{pmatrix}^T\begin{bmatrix}\mathbf{K_{qq}} & \mathbf{K_{qr}}\\ \mathbf{K_{rq}} & \mathbf{K_{rr}}\end{bmatrix}\begin{pmatrix}\mathbf{q}\\ \mathbf{r}\end{pmatrix} = \begin{pmatrix}\delta\mathbf{q}\\ \delta\mathbf{r}\end{pmatrix}^T\begin{pmatrix}\mathbf{Q}\\ \mathbf{R}\end{pmatrix} \tag{92}$$

where:

$$\begin{aligned}
\mathbf{K_{qq}} &= \mathbf{Q}\mathbf{Q} - \left(\mathbf{Q}\mathbf{P} + \tfrac{1}{2}\mathbf{T}\right)\mathbf{P}\mathbf{P}^{-1}\left(\mathbf{P}\mathbf{Q} + \tfrac{1}{2}\mathbf{U}\right)\\
\mathbf{K_{qr}} &= \mathbf{Q}\mathbf{R} - \left(\mathbf{Q}\mathbf{P} + \tfrac{1}{2}\mathbf{T}\right)\mathbf{P}\mathbf{P}^{-1}\left(\mathbf{P}\mathbf{R}\right)\\
\mathbf{K_{rq}} &= \mathbf{R}\mathbf{Q} - \left(\mathbf{R}\mathbf{P}\right)\mathbf{P}\mathbf{P}^{-1}\left(\mathbf{P}\mathbf{Q} + \tfrac{1}{2}\mathbf{U}\right)\\
\mathbf{K_{rr}} &= \mathbf{R}\mathbf{R} - \left(\mathbf{R}\mathbf{P}\right)\mathbf{P}\mathbf{P}^{-1}\left(\mathbf{P}\mathbf{R}\right)
\end{aligned} \tag{93}$$

As described before, the vector $\mathbf{Q}$ has the exact form of the generalized "force vector" in FEM, and $\delta\mathbf{q}^T\mathbf{Q}$ has the physical meaning of work done by force $\mathbf{Q}$ subjected to the displacement $\delta\mathbf{q}$ at the boundary S_b. We can also see that $\delta\mathbf{r}^T\mathbf{R}$ has the physical meaning of work done by force $\mathbf{R}$, which represents the crack surface tractions, subjected to the crack surface opening displacement $\delta\mathbf{r}$. If a traction free condition is considered at crack surfaces, the vector $\mathbf{R}$ vanishes and so does $\delta\mathbf{r}^T\mathbf{R}$.

8 Numerical Examples for SGBEM Super Element

8.1 Validation of SGBEM Super Elements

In this section, we test the performance of SGBEM Super Elements.

Firstly, we solve the problem of an embedded through-the-thickness crack. The same problem as in Fig. 5 is considered. One Super Element is used to solve this problem. The discretization of the Super Element includes 40 nodes at the outer boundary and 11 nodes at the crack. Computational results are shown in Tab. 9

$$K_1 = \sigma\sqrt{\pi a}\sqrt{\frac{2b}{\pi a}\tan\frac{\pi a}{2b}} \tag{94}$$

Table 8: Computational Results for the center crack in Fig. 5

	SGBEM	Analytical	Error
K1	28.65	28.50	0.53%

We also study the edge crack shown in Fig. 14. One Super Element is used to solve this problem. The discretization of the Super Element has 50 nodes at the outer boundary and 11 nodes at the crack. The computational results are compared to the handbook solution in Tab. 10

Table 9: Computational Results for the edge crack in Fig. 10

	SGBEM	Handbook	Error
K1	54.211	54.418	0.38%

We also study the case of a branching crack, as in Fig. 14. One Super Element is used to solve this problem. The discretization of the Super Element has 40 nodes at the outer boundary and 11 nodes at each crack segment.

Computational results are shown in Tab. 6.3, and are compared to those of [Chen and Hasebe (1995)].

Table 10: Computational Results for the branching crackshown in Fig. 14

	SGBEM	Chen and Hasebe (1995)	Error
F1A	0.964	0.964	0.00%
F1B	0.456	0.457	0.22%
F2B	0.469	0.467	0.43%

8.2 Implementation of the SGBEM Super-Element in to a FEM Code:

In this section, we implement the SGBEM Super Element into a standard finite element routine, for fracture and fatigue Analysis.

We also solve the problem of an embedded through-the-thickness slant crack as in Fig. 8. The same geometry and fatigue properties are considered. The mesh is shown in Fig. 17, with 100 finite elements and 1 Super Element. The Super Element contains 40 nodes at the outer boundary, and 11 nodes at the crack. The number of analysis steps is 30. The total crack increment = 0.3. Computation

results show that after 631138 cycles, the slant has grown to a mode I dominant crack as shown in Fig. 18. By comparing to the global SGBEM shown in section 7.1, we can see the final crack shape and fatigue cycles are very close. The fatigue cycle predicted by global SGBEM is 629398, which is slightly less the current result from Super Element.

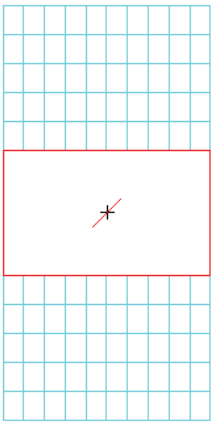

Figure 17: Mesh for the plate with an embedded slanted crack by FEM and Super Element, where the red color represents the Super Element

8.3 Using the SGBEM Super Element for Fatigue Analysis of Stiffened Aircraft Panels with Composite-Patches

In this example, we use SGBEM Super Element to analyze the fatigue growth of a center crack of thin panel with stiffeners and/or composite patches. Four cases are considered:

Case a: panel without stiffeners or composite patch

Case b: panel with 2 stiffeners only

Case c: panel with 1 composite patch only

Case d: panel with 2 stiffeners and 1 composite patch

A 250mm by 500mm panel is considered. A crack with initial length 25.7mm is located in the center of the panel.The length of each stiffener is 400 mm, and they are separated by a distance of 140 mm. The dimensions of the composite patch are 70mm by 100mm. The fibers of the composite patch are laid in the same direction of the tension applied to the upper and lower edges.

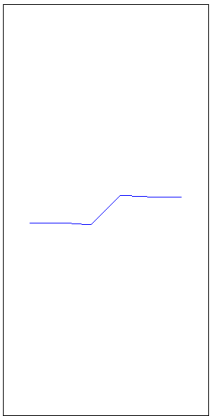

Figure 18: Final shape of the embedded slant crack, which grew by fatigue, byusing FEM and Super Element

Material properties are considered as:

Isotropic material for Panel: E=72.4 GPa, v =0.32, t =1mm.

Isotropic material for adhesive layer: E=1.07 GPa, v =0.32, t =0.127mm.

Orthotropic material for patch: E1=210 GPa, E2=25 GPa, G12=7.2 GPa, v12 =0.17, t =0.381mm.

Stiffeners: E=72.4 GPa, A=130 mm^2, I =4370mm^4.

The meshes of the panel, adhesive, patch and stiffeners are shown in Fig. 19-21. The panel is modeled with quadrilateral elements and one Super Element. The adhesive layer and the composite patch are modeled using quadrilateral elements. And the stiffeners are modeled by beam elements, with both translational and rotational degrees of freedoms.

A maximum uniform tension of 120Mpa is applied to the upper and the lower edge of the panel. Stress ratio of 0.1 is considered. Paris equation is used. The parameters of the equation are: C = 5.85×10^{-14} and n = 3.59. The number of analysis steps is 40. The total crack increment =40mm. So in each step the crack increment is 1mm. Predicted loading cycles are plotted against crack lengths in Fig. 22. As shown in the results, the order of the magnitude of fatigue lives for each case is such that: d>c>b>a, which is as expected.

We would like to point out that, the example in this study demonstrates that it is very simple and efficient to use the SGBEM super element to conduct fracture and

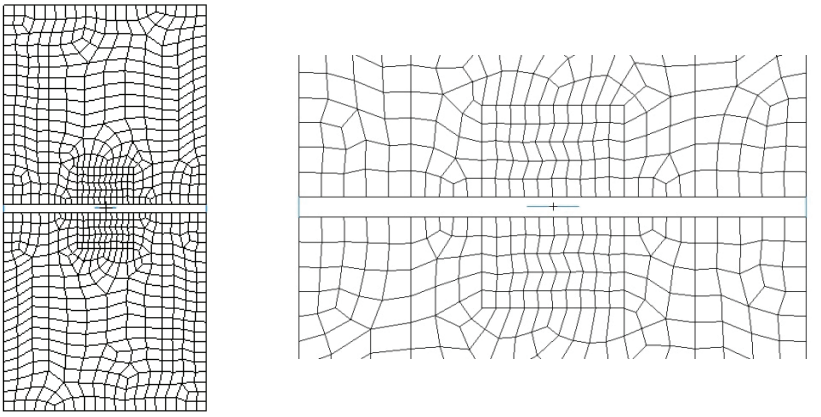

(a) (b)

Figure 19: (a) Mesh for the plate with center crack by quad elements and a Super Element, (b) a close-up view of the SGBEM Super Element

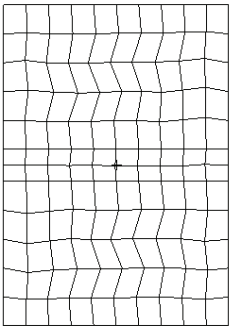

Figure 20: Mesh for the composite patch and the adhesive layer by using quad elements

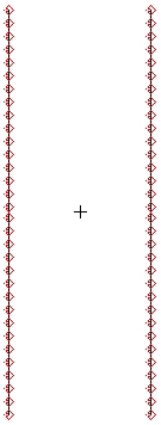

Figure 21: Mesh for the stiffeners by using beam elements

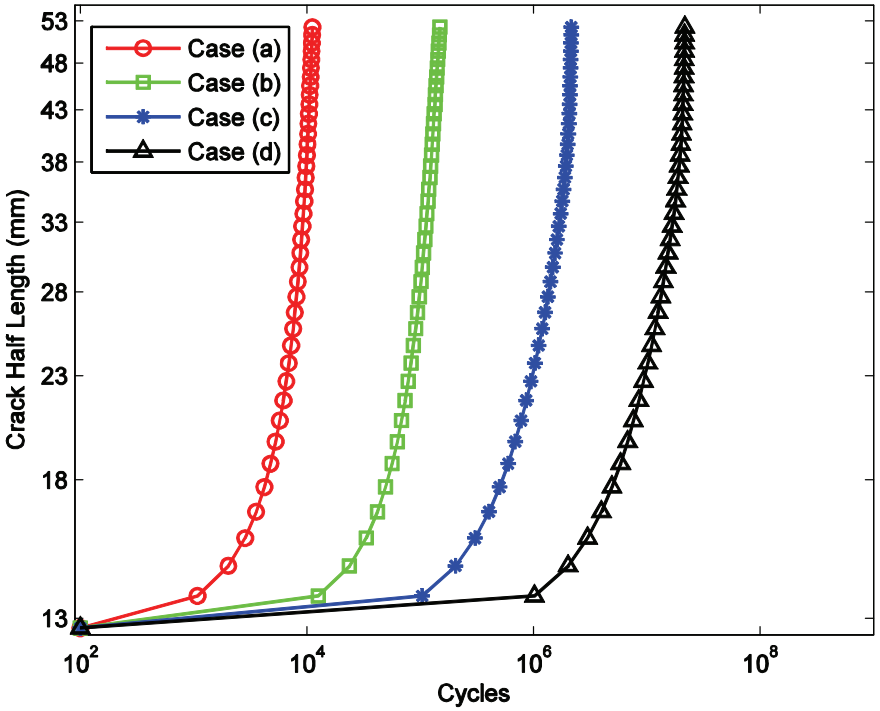

Figure 22: Predicted fatigue lives for the crack panel

fatigue analysis. However, quantitative comparisons of the computational results with real geometry and material properties, to their corresponding experimental results, will be carried out in future research.

9 Conclusion

Following the procedure of [Han and Atluri(2003)], 2D weakly-singular Symmetric Galerkin Boundary Elements (SGBEMs) are developed, and are used to calculate the stress intensity factors of arbitrary mixed mode, embedded, edge, branching, and intersecting cracks. Computed stress intensity factors show high accuracy, and the fatigue growth analysis of cracks requires minimal treatment, and no re-meshing.

A Super Element is developed by rearranging the symmetric Galerkin boundary integral equations. The Super Element is an arbitrarily-shaped domain with cracks inside it. Each Super Element has a stiffness matrix and a force vector, which have physical meanings similar to those by traditional finite elements. Likewise, the stiffness matrix of the Super Element is also positive semi-definite and has exactly three rigid body modes. Super Elements can be directly coupled with traditional finite elements or special elements, using the simple assembly procedures. This makes SGBEM Super Elements very suitable for analyzing large-scale structures and complex structures. Fatigue analysis of cracked thin aircraft panels with stiffeners and composite patches are presented, showing the simplicity and efficiency of using SGBEM Super Elements to model cracked composite structures.

We also would like to point out that, Super Elements can also be used to model micromechanical behavior of heterogeneous materials, or even the growth of the micro-cracks inside heterogeneous materials. These challenging studies will be presented in future.

Acknowledgement: This work was supported in parts by NAVAIR under an STTR program, and by the Vehicle Technology Division of the Army Research Labs. The support and encouragement of Mr. Nam Phan, Mr. Dy Le, and Mr. KishenGoel are thankfully acknowledged. The help of Dr. J.H. Park and Dr. Z.D. Han are also greatly appreciated. The first author would like to thank Dr. Cheng Wang and Dr. Wen Chen for their support and advice.

References

Atluri, S. N. (1975): On hybrid finite element models in solid mechanics. *Advances in Computer Methods for Partial Differential Equations,* R. Vichnevetsky (eds.), AICA, pp. 346-356.

Atluri, S.N. (2005): *Methods of Computer Modeling in Engineering and the Sciences, Vol. 1*, Tech Science Press.

Atluri, S. N.; Kobayashi, A. S.; Nakagaki M. (1975): An assumed displacement hybrid finite element model for linear fracture mechanics, *International Journal of Fracture*, vol. 11, no. 2, pp. 257-271.

Atluri, S. N. (1986): *Computational Methods in the mechanics of fracture*, North Holland, Amsterdam (also translated into Russian, Mir Publishers, Moscow).

Atluri, S. N. (1997): *Structural Integrity and Durability*, Tech Science Press, Forsyth.

Bishay, P. L.; Atluri, S. N. (2012): High-Performance 3D Hybrid/Mixed, and Simple 3D Voronoi Cell Finite Elements, for Macro- & Micro-mechanical Modeling of Solids, Without Using Multi-field Variational Principles, *CMES: Computer Modeling in Engineering & Sciences*, vol. 84, no. 1, pp. 41-98.

Bonnet, M.; Maier, G.; Polizzotto, C. (1998) Symmetric Galerkin boundary element methods.Applied Mechanics Review, vol. 51, pp. 669-704.

Chen, Y. Z.; Hasebe, N. (1995): New integration scheme for the branch crack problem. *Engineering Fracture Mechanics,* vol. 52, no. 5, pp. 791-801.

Dong, L.; Atluri, S. N. (2011a): A simple procedure to develop efficient & stable hybrid/mixed elements, and Voronoi Cell Finite Elements for macro- & micromechanics. *CMC: Computers, Materials & Continua*, vol. 24, no. 1, pp.61-104.

Dong, L.; Atluri, S. N. (2011b): Development of T-Trefftz four-node quadrilateral and Voronoi Cell Finite Elements for macro- & micromechanical modeling of solids. *CMES: Computer Modeling in Engineering & Sciences*, vol.81, no. 1, pp.69-118.

Dong, L.; Atluri, S. N. (2012a): T-Trefftz Voronoi Cell Finite Elements with eastic/rigid inclusions or voids for micromechanical analysis of composite and porous materials. *CMES: Computer Modeling in Engineering & Sciences*, vol.83, no. 2, pp.183-220.

Dong, L.; Atluri, S. N. (2012b): Development of 3D T-TrefftzVoronoi Cell Finite Elements with/without Spherical Voids &/or Elastic/Rigid Inclusions for Micromechanical Modeling of Heterogeneous Materials. CMC: *Computers, Materials & Continua*, vol. 29, no. 2, pp.169-212.

Dong, L.; Atluri, S. N. (2012c): Development of 3D Trefftz Voronoi Cells with Ellipsoidal Voids &/or Elastic/Rigid Inclusions for Micromechanical Modeling of Heterogeneous Materials. *CMC: Computers, Materials & Continua*, vol. 30, no. 1, pp.39-82.

Eshelby, J. D.(1951): The Force on an Elastic Singularity. *Philosophical Transac-*

tions of the Royal Society A: Mathematical, Physical & Engineering Sciences, vol. 244 no. 877, pp. 87-112.

Eshelby, J. D.(1975): The elastic energy-momentum tensor. *Journal of Elasticity*, vol. 5, no. 3-4, pp.321-335.

Frangi, A; Novati, G. (1996): Symmetric BE method in two-dimensional elasticity: evaluation of double integrals for curved elements, *Computational Mechanics*, vol. 19, issue 2. pp. 58-68.

Frangi, A; Novati, G.; Springhetti, R.; Rovizzi, M. (2002): 3D fracture analysis by the symmetric Galerk in BEM, *Computational Mechanics*, vol. 28, pp. 220-232.

Frangi, A.; Novati ,G. (2003): BEM-FEM coupling for 3D fracture mechanics applications. *Computational Mechanics*., vol. 32, pp. 415-422.

Han, Z. D..; Atluri, S. N. (2002): SGBEM (for Cracked Local Subdomain) – FEM(for uncracked global Structure) AlternatingMethod for Analyzing 3D Surface Cracks and Their Fatigue-Growth. *CMES: Computer Modeling in Engineering & Sciences*, vol.3, no.6, pp.699-716.

Han, Z. D.; Atluri, S. N. (2003): On Simple Formulations of Weakly-Singular Traction & Displacement BIE, andTheir Solutions through Petrov-Galerkin Approaches. *CMES: Computer Modeling in Engineering & Sciences*, vol. 4, no. 1, pp.5-20.

Henshell, R. D.; Shaw, K. G.(1975): Crack tip finite elements are unnecessary. *International Journal for Numerical Methods in Engineering* vol. 9, issue 3, pp. 495-507.

Li, S.; Mear, M.E.; Xiao, L. (1998): Symmetric weak form integral equation method for three-dimensional fracture analysis. *Computer Methods in Applied Mechanics and Engineering*, vol. 151, pp. 435-459.

Moes, N.; Dolbow J.; Belytschko T. (1999): A finite element method for crack growth without remeshing. *International Journal for Numerical Methods in Engineering*, vol. 46, pp. 131-150.

Murakami, K. (1987):*Stress Intensity Factors Handbook*.Pergamon Press, Oxford

Nishioka, T.; Atluri, S.N. (1982): Analytical solution for embedded elliptical cracks and finite element alternating method for elliptical surface cracks, subjected to arbitrary loadings. *Engineering Fracture Mechanics*, vol. 17, pp. 247-268.

Nishioka, T.; Atluri, S. N. (1983): Path-independent integrals, energy release rates, and general solutions of near-tip fields in mixed-mode dynamic fracture mechanics. *Engineering Fracture Mechanics*, vol. 18, issue 1, pp.1-22.

Nikishkov, G.P.; Atluri, S.N. (1987): Calculation of fracture mechanics parameters for an arbitrary three-dimensional crack by the equivalent domain integral

method. *International Journal of Numerical Methods in Engineering*, vol. 24, pp. 851-867.

Nikishkov, G. P..; Park, J. H.; Atluri, S. N. (2001): SGBEM-FEM alternating method for analyzing 3D non-planar cracks and their growth in structural components. *CMES: Computer Modeling in Engineering & Sciences*, vol.2, no.3, pp.401-422.

Okada, H.; Rajiyah, H.; Atluri, S. N. (1988): A Novel Displacement Gradient Boundary Element Method for Elastic Stress Analysis with High Accuracy, *Journal of Applied Mechanics*, vol. 55, pp. 786-794.

Okada, H.; Rajiyah, H.; Atluri, S. N. (1989): Non-hyper-singular integral representations for velocity (displacement) gradients in elastic/plastic solids (small or finite deformations), *Computational Mechanics.*, vol. 4, no. 3, pp. 165-175.

Park, J. H.; Atluri, S. N. (1998): Mixed mode fatigue growth of curved cracks emanating from fastener holes in aircraft lap joints. *Computational Mechanics*, vol. 21, issue 6, pp. 1333-1336.

Pian, T. H. H. (1964): Derivation of element stiffness matrices by assumed stress distribution. *A. I. A. A. Journal*, vol. 2, pp. 1333-1336.

Rice, J. R. (1968): A path independent integral and the approximate analysis of strain concentration by notches and cracks. ASME: *Journal of Applied Mechanics*, vol. 35, issue 2, pp. 379-386.

Tong, P; Pian, T. H. H; Lasry, S. J. (1973): A hybrid-element approach to crack problems in plane elasticity. *International Journal for Numerical Methods in Engineering, vol. 7, issue 3, pp. 297-308.*

Vijayakumar, K; Atluri, S. N. (1981): An embedded elliptical crack, in an infinite solid, subject to arbitrary crack-face tractions. *ASME, Journal of Applied Mechanics,* vol. 103, no. 1, pp. 88-96.